NACA RM A57I10

NACA

RESEARCH MEMORANDUM

EFFECTS OF VERTICAL LOCATION OF WING AND HORIZONTAL TAIL ON THE AERODYNAMIC CHARACTERISTICS IN PITCH AT MACH NUMBERS FROM 0.60 TO 1.40 OF AN AIRPLANE CONFIGURATION WITH AN UNSWEPT WING

By Louis S. Stivers, Jr., and Garth W. Lippmann

Ames Aeronautical Laboratory
Moffett Field, Calif.

NATIONAL ADVISORY COMMITTEE
FOR AERONAUTICS

WASHINGTON

November 20, 1957

NACA RM A57I10

NATIONAL ADVISORY COMMITTEE FOR AERONAUTICS

RESEARCH MEMORANDUM

EFFECTS OF VERTICAL LOCATION OF WING AND HORIZONTAL TAIL ON THE AERODYNAMIC CHARACTERISTICS IN PITCH AT MACH NUMBERS FROM 0.60 TO 1.40 OF AN AIRPLANE CONFIGURATION WITH AN UNSWEPT WING

By Louis S. Stivers, Jr., and Garth W. Lippmann

SUMMARY

An experimental investigation was conducted to determine the effects of vertical location of an unswept wing and horizontal tail on the aerodynamic characteristics in pitch of a wing-body-tail combination. The wing had an aspect ratio of 3.09, a taper ratio of 0.39, the quarter-chord line swept back 11.5°, and biconvex sections. Lift, drag, and pitching-moment coefficients were obtained at Mach numbers from 0.60 to 1.40 for angles of attack from -4° to approximately 13°, with the boundary-layer transition on the model fixed and free. The Reynolds number of the tests was 1.5 million, based on the wing mean aerodynamic chord. The effects of Mach number on the experimental and calculated lift curve slopes, pitching-moment curve slopes, and contributions of the horizontal tail to the pitching-moment curve slopes are presented for the various wing and horizontal-tail locations.

INTRODUCTION

One of many aerodynamic problems confronting the designer of transonic or supersonic aircraft having a horizontal tail is that of locating this tail to provide satisfactory static longitudinal stability throughout the expected ranges of flight speed and attitude. Usually, existing theory is not able to provide sufficiently reliable information for the designer, and the only recourse is to experiment. Only in exceptional cases, however, is the configuration of a proposed airplane sufficiently similar to that of a tested model that the experimental data can be employed directly. Usually, the designer must depend on an interpolation of results for a

number of related configurations. Reliable information is provided in this manner, however, only when enough experimental data are available to bracket the contemplated values of each design parameter.

For unswept-wing configurations, a summary of some horizontal-tail data obtained at low subsonic Mach numbers is available in reference 1, and the results of several distinct investigations at transonic Mach numbers are reported in references 2 to 13. These latter results, however, provide little information on the effects of vertical location of the horizontal tail.

The purpose of the present report is to provide some of the necessary data for locating the horizontal tail on unswept-wing airplanes so as to furnish desirable longitudinal stability characteristics at transonic Mach numbers. The data were obtained from an investigation, throughout the transonic Mach number range, of the effects of vertical location of the wing and horizontal tail on the lift, drag, and pitching-moment characteristics of an airplane configuration having an unswept, tapered wing of aspect ratio 3.09. The investigation was conducted in the Ames 2- by 2-foot transonic wind tunnel for Mach numbers from 0.60 to 1.40, for angles of attack as high as about 13°, and for a Reynolds number of 1.5×10^6, based on the mean aerodynamic chord of the wing. Theoretical values of lift and pitching-moment curve slopes together with the contributions of the horizontal tail to the pitching-moment curve slopes, calculated by the methods of reference 14, are presented for comparison with the corresponding experimental values. All the data reported herein are presented without discussion.

NOTATION

b	wing span
C_D	drag coefficient
C_L	lift coefficient
C_{L_α}	lift curve slope, $\frac{\partial C_L}{\partial \alpha}$
C_m	pitching-moment coefficient referred to $\frac{\bar{c}}{4}$ (See fig. 1.)
$C_{m_{C_L}}$	pitching-moment curve slope, $\frac{\partial C_m}{\partial C_L}$

[redacted]

$\Delta\left(C_{m_{C_L}}\right)_{tail}$ contribution of the horizontal tail to the pitching-moment curve slope, $\left(C_{m_{C_L}}\right)_{tail\ on} - \left(C_{m_{C_L}}\right)_{tail\ off}$ at constant α

c local chord of wing

c_t local chord of horizontal tail

$\bar{c}$ mean aerodynamic chord of wing

$\bar{c}_t$ mean aerodynamic chord of horizontal tail

M free-stream Mach number

z vertical distance above the wing chord plane

α angle of attack, deg

APPARATUS AND TEST PROCEDURE

Model

The configuration of the basic model with pertinent dimensions and data are given in figure 1(a). The model was made of steel and, to facilitate changes in configuration, was constructed in three parts: the body-nose unit, the wing unit which included the middle portion of the body, and the tail unit which included the afterbody. Two wing units were made: one with the wing in a plane passing through the body axis (hereinafter designated mid wing) and one with the wing high on the body (high wing). The wing was uncambered and untwisted and was fixed on the body at zero incidence with no dihedral. Four tail units were made: an afterbody with neither horizontal nor vertical tails (tail off), one including both horizontal and vertical tails with the horizontal tail in a plane passing through the body axis (mid tail), and one each with the horizontal tail in a moderately high (moderately high tail) and a high location (high tail) supported by a swept, untapered strut. The vertical tail and the struts had NACA 0003 airfoil sections in the streamwise direction. The tails were all fixed at zero incidence with no dihedral. The wing and tail units were made in such a manner that the span and longitudinal location of the wing and horizontal tail remained fixed for the different vertical locations. Furthermore, the high-wing and high-tail units could be rotated through an angle of 180° to form low-wing or low-tail configurations.

A total of ten configurations was employed in the present investigation. In the following table these configurations are listed together with the appropriate values of the horizontal tail-height parameter, $z/(b/2)$.

Configurations	$\frac{z}{b/2}$
Mid wing, tail off	---
Low wing, tail off	---
High wing, tail off	---
Mid wing, mid tail	0
Mid wing, moderately high tail	0.16
Mid wing, high tail	0.33
Mid wing, moderately low tail	-0.16
Mid wing, low tail	-0.33
Low wing, high tail	0.45
High wing, moderately low tail	-0.28

The arrangement and principal dimensions of the various wing and tail configurations employed in the present investigation are illustrated in figure 1(b).

Wind Tunnel and Model-Support System

The Ames 2- by 2-foot transonic wind tunnel, in which the present tests were conducted, utilizes a flexible nozzle and porous test-section walls, as illustrated in figure 2, to permit continuous operation to a Mach number as high as 1.4 and to provide choke-free flow in the test section throughout the transonic Mach number range. The stagnation pressure within the wind tunnel can be varied to maintain a constant Reynolds number throughout the operational range of Mach numbers. A detailed decription of the tunnel and of the function of various component parts is presented in reference 15.

During the tests the model was mounted in the wind-tunnel test section on a 1-inch-diameter, flexure-type, sting-supported balance. This balance was enclosed within the body of the model and was fitted with electrical-resistance strain gages with which the forces and moments on the model were measured. A model mounted on the sting-supported balance is shown in figure 3. The sting-support housing can be inclined through an angle-of-attack range of -8° to 8° in a fixed plane, with the center of rotation located near the middle of the model. A 4° bent sting was employed for the present tests in order to provide an angle-of-attack range of -4° to 12°, neglecting deflections due to wind loads.

[redacted]

Tests

Lift, drag, and pitching-moment data were obtained at 20 Mach numbers ranging from 0.60 to 1.40 and at angles of attack ranging from -4° to approximately 13° for the configurations and conditions of boundary-layer transition checked in the following table. (Unreliable drag data were obtained for some configurations and are not presented.)

Configurations	Transition free			Transition fixed		
	Lift	Drag	Pitching moment	Lift	Drag	Pitching moment
Mid wing, tail off	X		X	X	X	X
Low wing, tail off	X	X	X	X	X	X
High wing, tail off	X	X	X			
Mid wing, mid tail	X		X	X	X	X
Mid wing, moderately high tail	X		X			
Mid wing, high tail	X		X	X	X	X
Mid wing, moderately low tail	X		X			
Mid wing, low tail	X		X			
Low wing, high tail	X	X	X	X	X	X
High wing, moderately low tail	X	X	X			

When either the loads on the balance or the power supplied to the wind-tunnel drive reached limiting values, the angle-of-attack range was correspondingly limited. The Reynolds number of the tests was held constant at a value of 1.5 million, based on the wing mean aerodynamic chord, except for the low-wing, tail-off and low-wing, high-tail configurations for a Mach number of 1.40 when the Reynolds number was decreased to 1.0 million to reduce the loads on the balance.

Boundary-layer transition was fixed on the wing and horizontal tail by means of a 0.005-inch-diameter wire attached to the surfaces along rays from the leading-edge apex to the quarter-chord points at the tips. Transition was not fixed on the vertical tail or on the vertical support struts. On the body, transition was fixed by a ring of 0.005-inch-diameter wire around the nose at a location 1.33 inches from the apex. A visualization technique showed that the boundary layer on the model became turbulent immediately downstream of the wire at low angles of attack over the Mach number range of the tests.

The increment in drag coefficient due to the transition wires could not be accurately evaluated from the data of the present investigation. It was estimated, however, that the increment for transition wires on the body nose and on both surfaces of the wing and horizontal tail varied from 0.0012 to 0.0015 over the test range of Mach numbers, and for wires only on the wing, from 0.0007 to 0.0009. For the estimations, the drag of

the wires was assumed to be due principally to pressure differences across the upstream and downstream sides of the wires. Pressures measured on forward and rearward facing steps, and obtained from reference 16 and from unpublished investigations in the Ames 1- by 3-foot and 1- by 3-1/2-foot wind tunnels, were employed in the calculations. It is significant to note that the pressures on the steps varied substantially depending on whether the boundary layer at the steps was laminar, transitional, or turbulent. For low supersonic Mach numbers the pressure differences across the faces of a step simulating a wire were roughly twice as much for a turbulent boundary layer as for a laminar boundary layer. For the above estimations, pressures were used that most nearly corresponded to the local boundary-layer conditions and local Reynolds and Mach numbers at the position of the transition wires on the model. (The boundary layer ahead of the wires was laminar and transition occurred at a distance behind the wires of the order of 10 wire diameters.) The above method of estimating the drag of the wires has been substantiated for the condition of a turbulent boundary layer over the wires. For this condition, increments in drag coefficient due to the wires were determined experimentally in the wind tunnel simply by adding a second wire on the wing parallel to and 1/4-inch downstream of the initial transition wire. The experimental increment in drag coefficient due to the second wire varied from 0.0011 to 0.0022 over the Mach number range from 0.60 to 1.40, whereas the corresponding estimated increments varied from 0.0013 to 0.0018.

CORRECTIONS AND PRECISION

Wall-interference corrections to the data of the present investigation have been neglected for both subsonic and supersonic Mach numbers. That the effects of the wind-tunnel walls are small is shown by the data of reference 15.

Various other factors which could influence the measured data have been considered and have been dealt with in various ways. Stream angularity corrections were insignificant, air-stream condensation effects were negligible, aeroelastic distortion of the wing and tail was believed to be small, and the influence of the sting support on the measured data was believed to be negligible. Consequently, corrections for these effects were not made. Each angle of attack, however, has been corrected for the deflection of the support sting and balance due to wind loads on the model. The axial forces measured by the internal balance have been adjusted to correspond to a condition of free-stream static pressure at the base of the body. The drag data presented in this report for the fixed-transition condition include the drag of the transition wires.

In addition to small systematic errors which may be introduced by the corrections that have been disregarded, the test data are subject to random errors of measurement which affect the precision of the data. An

analysis, based on the procedures of reference 17, has been made of the precision of Mach number, lift, drag, and pitching-moment coefficients, angle of attack, and Reynolds number for the present tests. These random uncertainties are given in the following table for low and moderate angles of attack and for three representative Mach numbers:

Item	M = 0.60		M = 1.00		M = 1.40	
	$\alpha = 0.25^\circ$	$\alpha = 6^\circ$	$\alpha = 0.25^\circ$	$\alpha = 6^\circ$	$\alpha = 0.25^\circ$	$\alpha = 6^\circ$
M	±0.002	±0.002	±0.002	±0.002	±0.002	±0.002
C_L	±.004	±.005	±.002	±.007	±.001	±.005
C_m	±.003	±.004	±.002	±.007	±.001	±.005
C_D	±.0002	±.0004	±.0002	±.0011	±.0002	±.0010
α	±.02°	±.01°	±.02°	±.03°	±.02°	±.02°
R	$\pm.03\times10^6$	$\pm.03\times10^6$	$\pm.02\times10^6$	$\pm.02\times10^6$	$\pm.08\times10^6$	$\pm.08\times10^6$

RESULTS

The lift, drag, and pitching-moment data have been reduced to standard coefficient form using wing area, including the portion covered by the body, as the reference area. Pitching-moment coefficients for each configuration are based on the wing mean aerodynamic chord and are referred to a point on the body axis, the longitudinal position of which corresponds to the 25-percent point of the wing mean aerodynamic chord (see fig. 1).

The results included in this report are presented without discussion. The variations of lift coefficient with angle of attack, pitching-moment coefficient, and drag coefficient with lift coefficient are presented in figures 4 to 9 for the configurations with tail on and off. The lift, pitching-moment, and drag data are given, respectively, in figures 4, 6, and 8 for boundary-layer transition free and in figures 5, 7, and 9 for transition fixed. In order to distinguish among the pitching-moment data at high lift coefficients for Mach numbers of 0.80, 0.85, and 0.90, flags have been added to the symbols for a Mach number of 0.85. Portions of the curves at a Mach number of 1.40 for the low-wing, tail-off and low-wing, high-tail configurations have been broken to indicate that these parts of the curves correspond to a Reynolds number of 1.0 million. The effect of Mach number on C_{L_α} and $C_{m_{C_L}}$ at lift coefficients of 0, 0.2, and 0.4, transition both fixed and free, are presented in figures 10 and 11 for wing-body and wing-body-tail combinations, respectively. Calculated values of C_{L_α} and $C_{m_{C_L}}$ determined by the methods of reference 14 are also shown in figures 10 and 11 for comparison with the experimental values at a lift coefficient of zero. Contributions of the horizontal tail to $C_{m_{C_L}}$ at

[redacted]

lift coefficients of 0, 0.2, and 0.4 are shown in figures 12 and 13 for transition free and fixed, respectively. Both calculated and experimental values of the horizontal-tail contributions to $C_{m_{C_L}}$ at zero lift coefficient are presented in figure 14 for comparison.

For the calculations of C_{L_α}, $C_{m_{C_L}}$, and the contribution of the horizontal tail to $C_{m_{C_L}}$ by the methods of reference 14, theoretical wing alone lift curve slopes were utilized as determined for subsonic, sonic, and supersonic Mach numbers by the methods of references 18, 19, and 20, respectively. Inasmuch as the effect of changing the position of the wing of the present wing-body combination is believed to be within the accuracy of the calculations, the calculated slopes for the mid-wing configuration are also taken as those for the low-wing and high-wing configurations. The calculations involving the high (or low) tail were determined assuming zero interference between the tail and the body. The interference on the moderately high (or moderately low) tail due to the wing and due to the body, however, could not be determined directly from reference 14. To determine this interference, downwash distributions across the tail due to the wing vortices and due to the cross-flow-velocity component over the body were calculated. These downwash distributions were used to compute the ratios of interference lift to the lift of the tail alone by means of the Alden-Schindel technique described in reference 14, with the simplification that the reverse-flow spanwise-lift distribution was elliptical.

Ames Aeronautical Laboratory
National Advisory Committee for Aeronautics
Moffett Field, Calif., Sept. 10, 1957

REFERENCES

1. Neely, Robert H., and Griner, Roland F.: Summary and Analysis of Horizontal-Tail Contribution to Longitudinal Stability of Swept-Wing Airplanes at Low Speeds. NACA RM L55E23a, 1955.

2. Goodson, Kenneth W., and Becht, Robert E.: Wind-Tunnel Investigation at High Subsonic Speeds of the Static Longitudinal Stability Characteristics of a Complete Model Having Cropped-Delta, Swept, and Unswept Wings and Several Horizontal-Tail Heights. NACA RM L54H12, 1954.

3. Smith, Willard G.: Wind-Tunnel Investigation at Subsonic and Supersonic Speeds of a Fighter Model Employing a Low-Aspect-Ratio Unswept Wing and a Horizontal Tail Mounted Well Above the Wing Plane - Longitudinal Stability and Control. NACA RM A54D05, 1954.

[redacted]

4. Sleeman, William C., Jr.: An Experimental Study at High Subsonic Speeds of Several Tail Configurations on a Model With an Unswept Wing. NACA RM L56A06a, 1956.

5. Gillis, Clarence L., and Vitale, A. James: Wing-On and Wing-Off Longitudinal Characteristics of an Airplane Configuration Having a Thin Unswept Tapered Wing of Aspect Ratio 3, as Obtained From Rocket-Propelled Models at Mach Numbers From 0.8 to 1.4. NACA RM L50K16, 1951.

6. McFall, John C., Jr., and Hollinger, James A.: Longitudinal Stability, Control Effectiveness, and Drag Characteristics at Transonic Speeds of a Rocket-Propelled Model of an Airplane Configuration Having an Unswept Tapered Wing of Aspect Ratio 3.0 and NACA 65A004.5 Airfoil Sections. NACA RM L52L04, 1953.

7. White, Maurice D.: A Flight Investigation at Transonic Speeds of the Aerodynamic Characteristics of a Model Having a Thin Unswept Wing of Aspect Ratio 3.1. NACA RM A54E12, 1954.

8. Kehlet, Alan B.: Aerodynamic Characteristics at Transonic and Supersonic Speeds of a Rocket-Propelled Airplane Configuration Having a Diamond-Plan-Form Wing of Aspect Ratio 3.08 and a Low, Swept Horizontal Tail. NACA RM L54G27a, 1954.

9. Gillespie, Warren, Jr.: Lift, Drag, and Longitudinal Stability at Mach Numbers From 0.8 to 2.1 of a Rocket-Powered Model Having a Tapered Unswept Wing of Aspect Ratio 3 and Inline Tail Surface. NACA RM L55B10, 1955.

10. Summers, James L., Treon, Stuart L., and Graham, Lawrence A.: Effects of Taper Ratio on the Longitudinal Characteristics at Mach Numbers From 0.6 to 1.4 of a Wing-Body-Tail Combination Having an Unswept Wing of Aspect Ratio 3. NACA RM A54L20, 1955.

11. Hieser, Gerald, and Kudlacik, Louis: Longitudinal Aerodynamic Characteristics at Transonic Speeds of a Complete Model With an Unswept Wing and a Sweptback Horizontal Tail at Two Vertical Locations. NACA RM L55F30, 1955.

12. Morse, D. S., Hey, W. A., Bicknell, J., and Parsons, T. R.: Wind Tunnel Measurement of Static Stability and Control Characteristics of Representative Supersonic Interceptor Airplanes at Mach Numbers From 0.8 to 1.2. TACP Rep. No. 12, MIT Aero. Eng. Dept., Mar. 1955.

13. Summers, James L., Treon, Stuart L., and Graham, Lawrence A.: Wind-Tunnel Investigation at Mach Numbers From 0.8 to 1.4 of Static Longitudinal and Lateral-Directional Characteristics of an Unswept-Wing Airplane Model. NACA RM A56E22, 1956.

[redacted]

14. Nielsen, Jack N., Kaattari, George E., and Anastasio, Robert F.: A Method for Calculating the Lift and Center of Pressure of Wing-Body-Tail Combinations at Subsonic, Transonic, and Supersonic Speeds. NACA RM A53G08, 1953.

15. Spiegel, Joseph M., and Lawrence, Leslie F.: A Description of the Ames 2- by 2-Foot Transonic Wind Tunnel and Preliminary Evaluation of Wall Interference. NACA RM A55I21, 1955.

16. Chapman, Dean R., Kuehn, Donald M., and Larson, Howard K.: Investigation of Separated Flows in Supersonic and Subsonic Streams With Emphasis on the Effect of Transition. NACA TN 3869, 1957.

17. Beers, Yardley: Introduction to the Theory of Error. Addison-Wesley Publishing Co., Cambridge, Mass., 1953.

18. DeYoung, John, and Harper, Charles W.: Theoretical Symmetric Span Loading at Subsonic Speeds for Wings Having Arbitrary Plan Form. NACA Rep. 921, 1948.

19. Spreiter, John R.: Aerodynamic Properties of Slender Wing-Body Combinations at Subsonic, Transonic, and Supersonic Speeds. NACA Rep. 962, 1948. (Supersedes NACA TN's 1662 and 1897)

20. Lapin, Ellis: Charts for the Computation of Lift and Drag of Finite Wings at Supersonic Speeds. Rep. SM-13480, Douglas Aircraft Co., Inc., Oct. 1949.

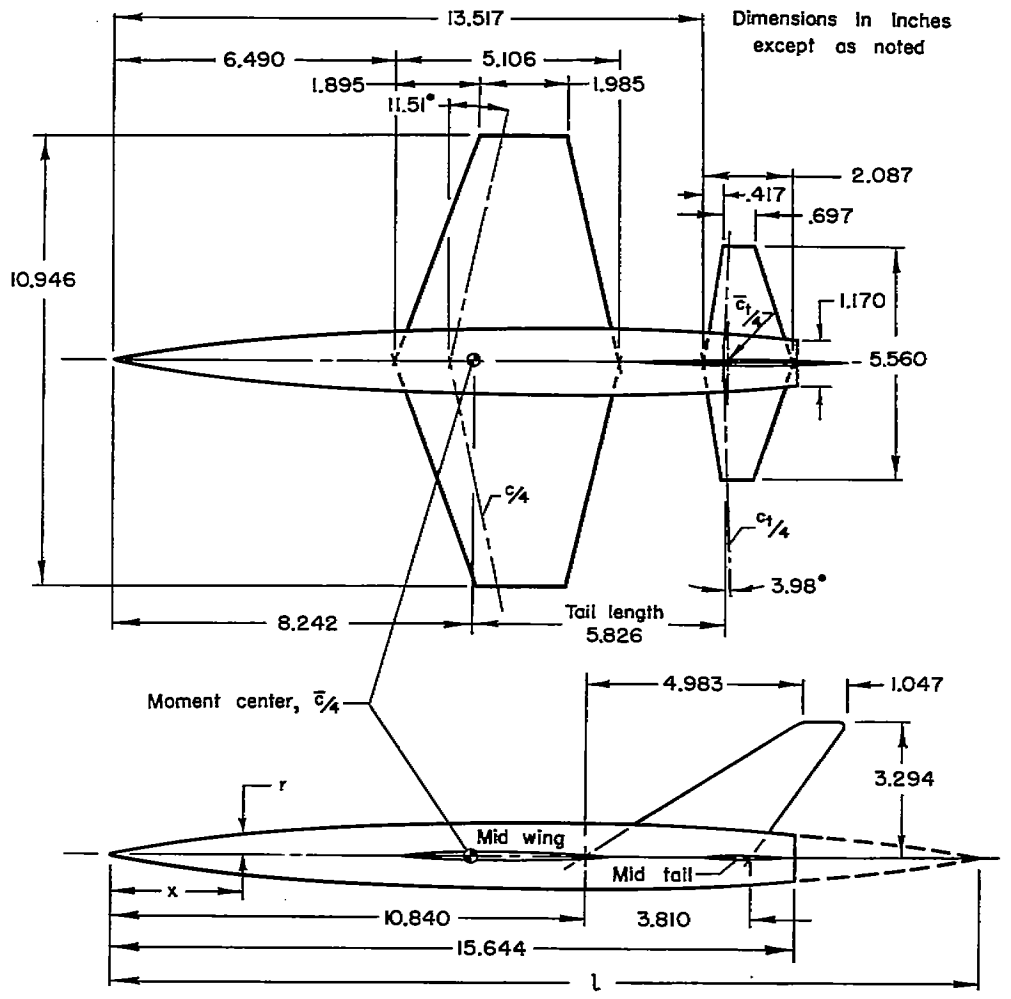

	Wing	Horizontal tail
Aspect ratio	3.09	3.99
Taper ratio	.39	.33
Thickness-chord ratio	.03	.03
Airfoil section	Biconvex	Circular arc (max. thickness at 0.3 chord)
Area	38.81 sq in.	7.74 sq in.
Mean aerodynamic chord	3.77 in.	1.51 in.
Location of unswept line	.61 c	.30 c_t

Body

Ordinates given by:

$$\frac{r}{r_o} = \left[1-\left(1-\frac{2x}{l}\right)^2\right]^{\frac{3}{4}}$$

Where:

r = local radius

$r_o = r_{maximum} = 0.794$

x = longitudinal distance from nose

$l = 2(x_{for\ r_o}) = 19.833$

(a) Basic model with horizontal tail located in the middle position.

Figure 1.- Configurations of the model investigated.

[redacted]

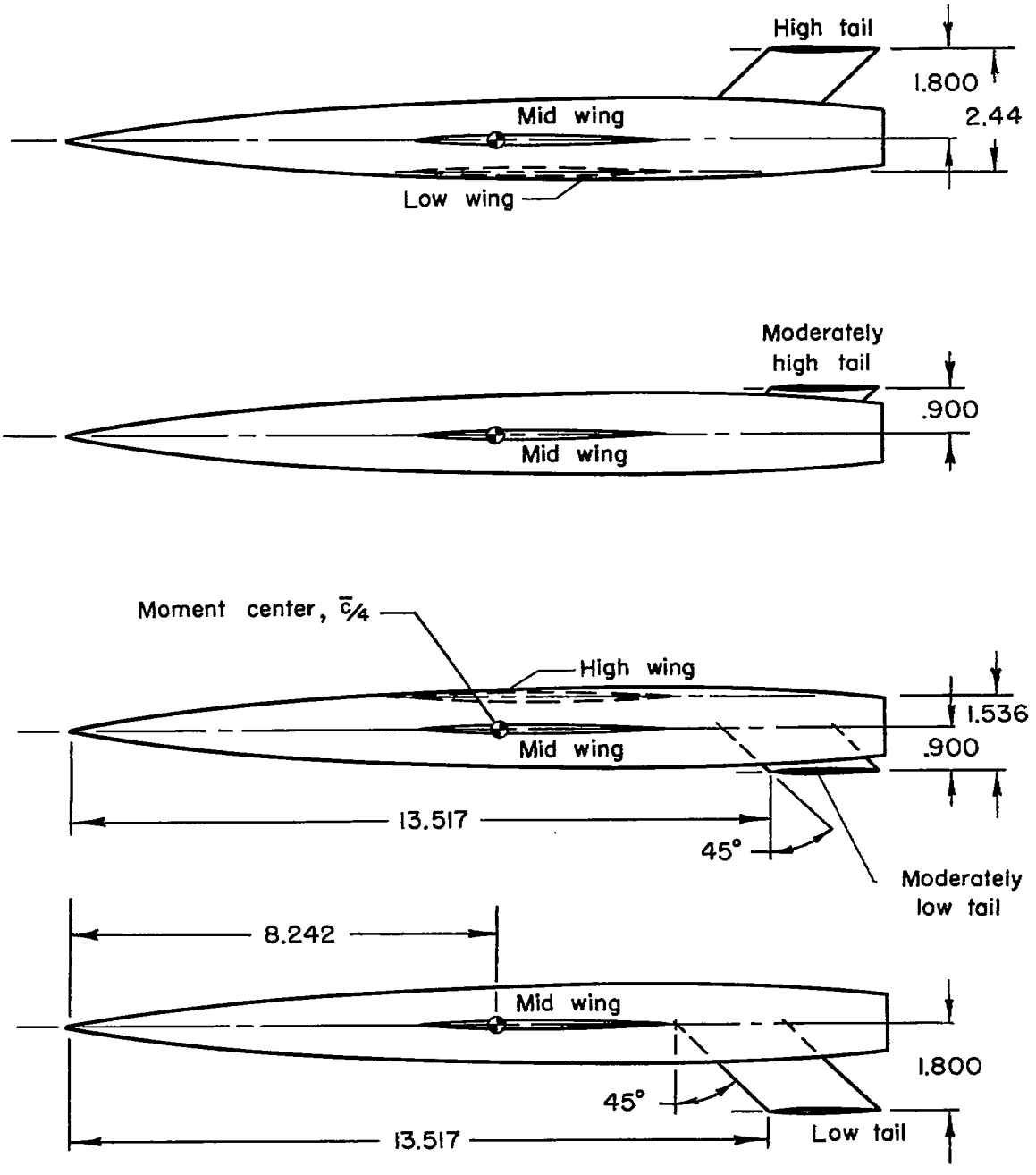

(b) Locations of the horizontal tail above and below the chord plane of the wing extended.

Figure 1.- Concluded.

[redacted]

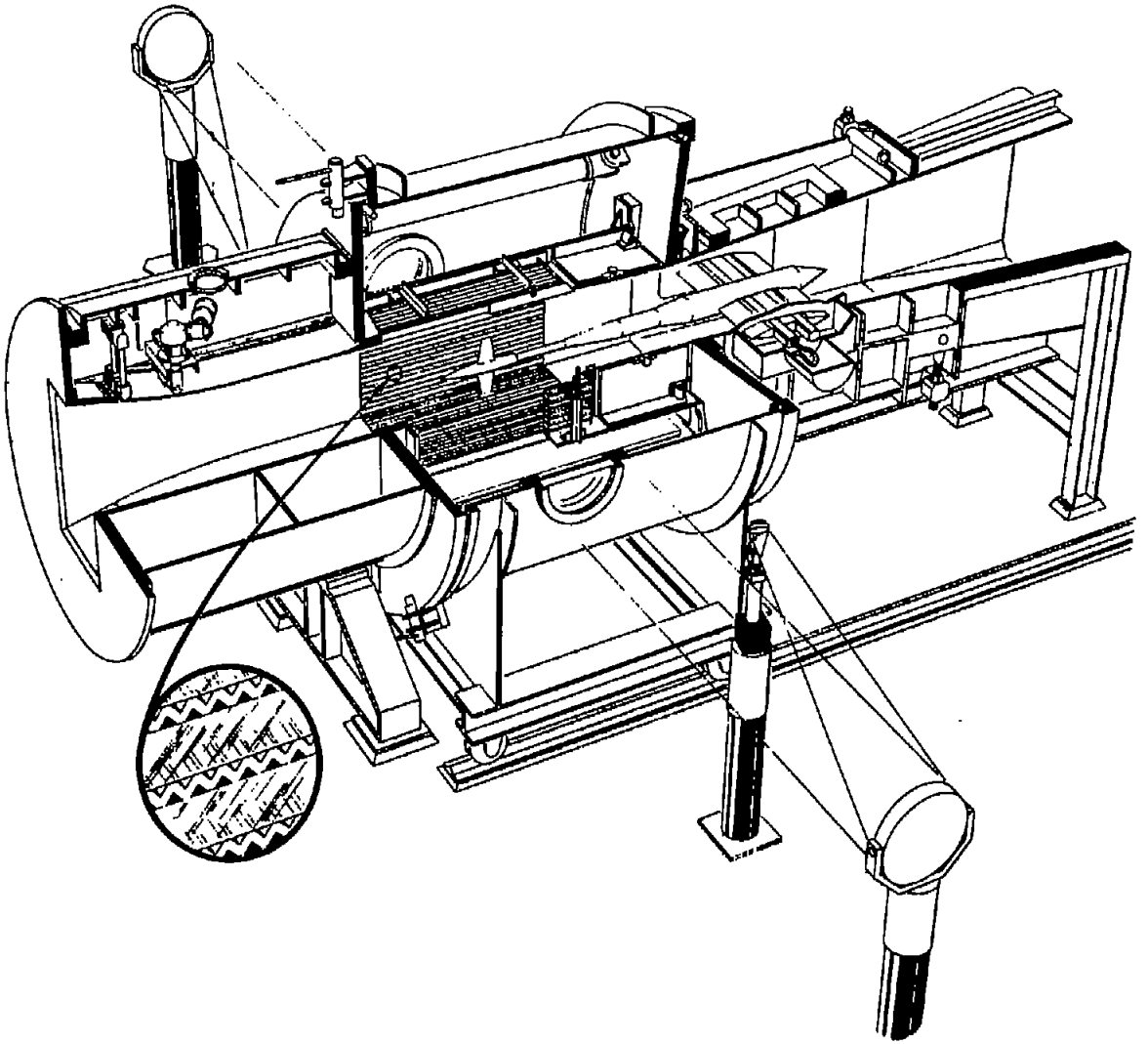

Figure 2.- Diagram of the test region of the Ames 2- by 2-foot transonic wind tunnel.

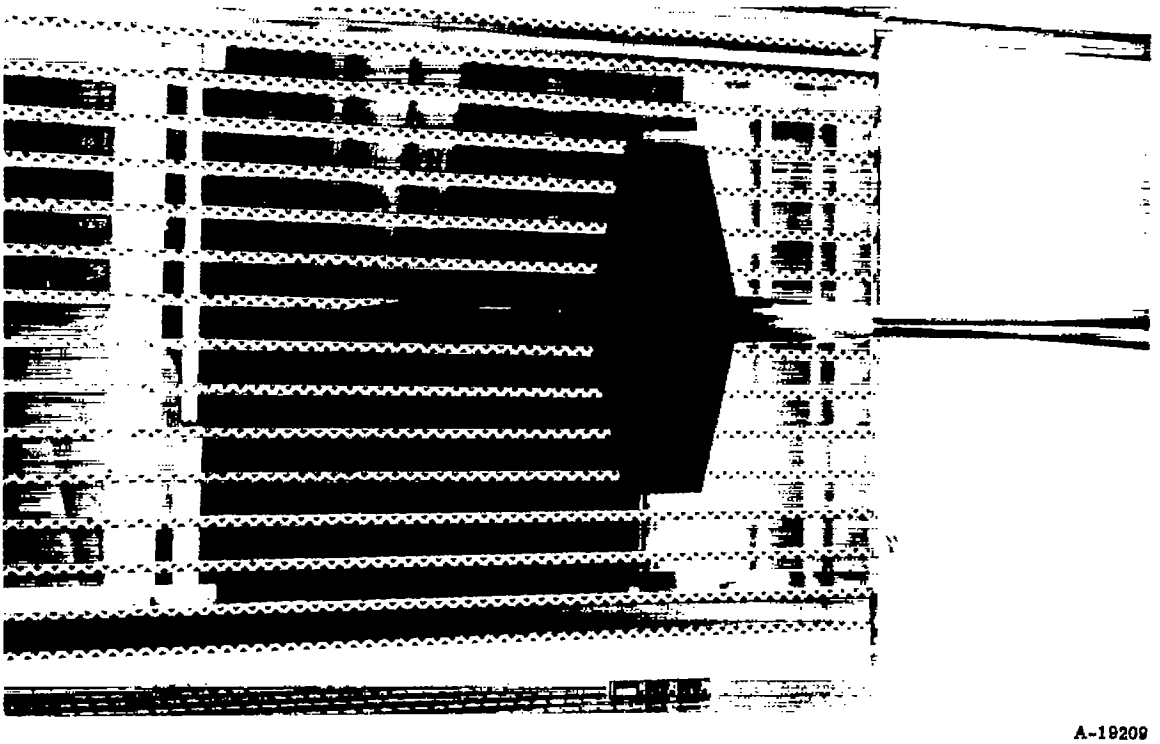

A-19209

Figure 3.- Typical model installation in the Ames 2- by 2-foot transonic wind tunnel.

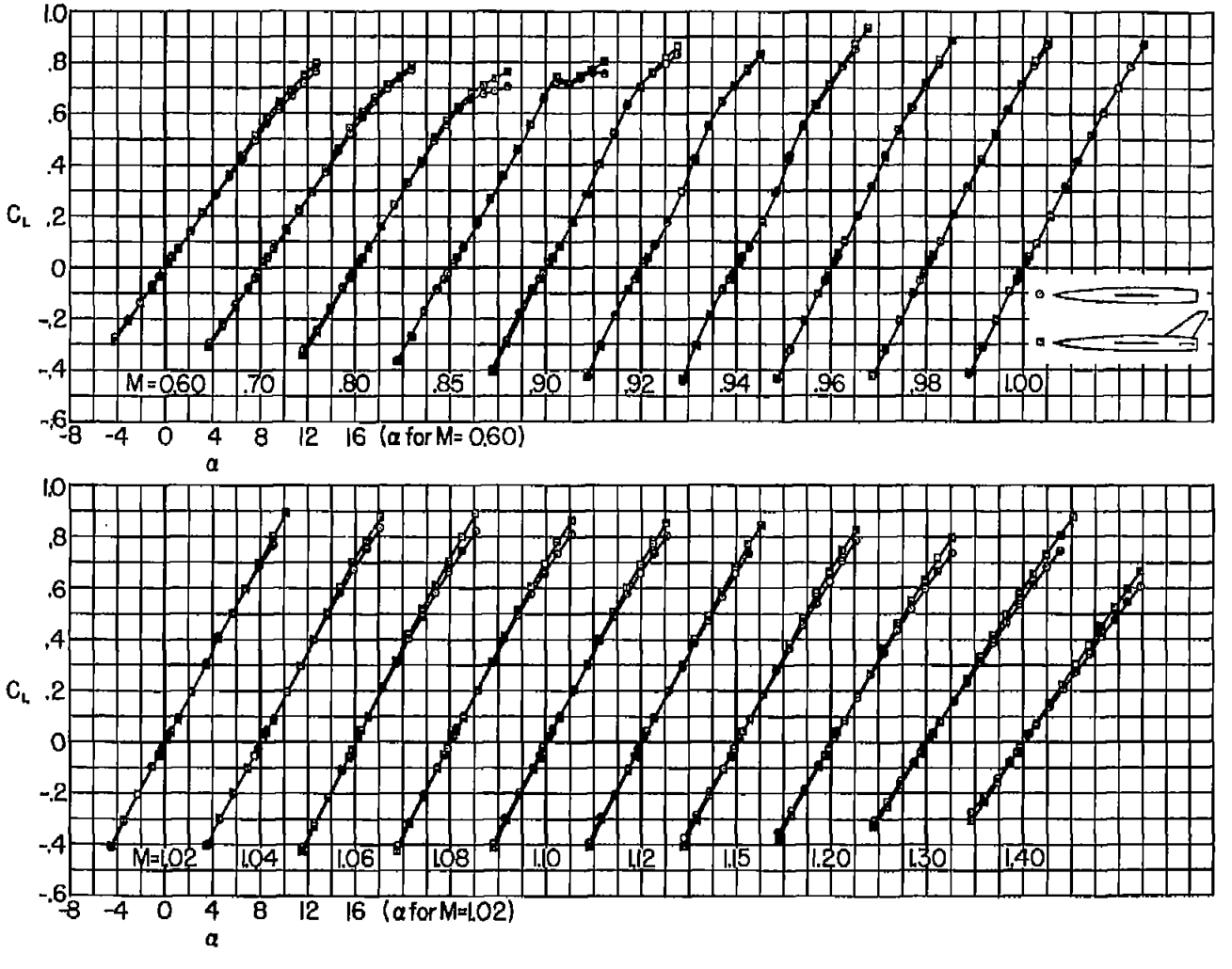

(a) Mid-wing, mid-tail configuration.

Figure 4.- Variation of lift coefficient with angle of attack for constant Mach number; boundary-layer transition free.

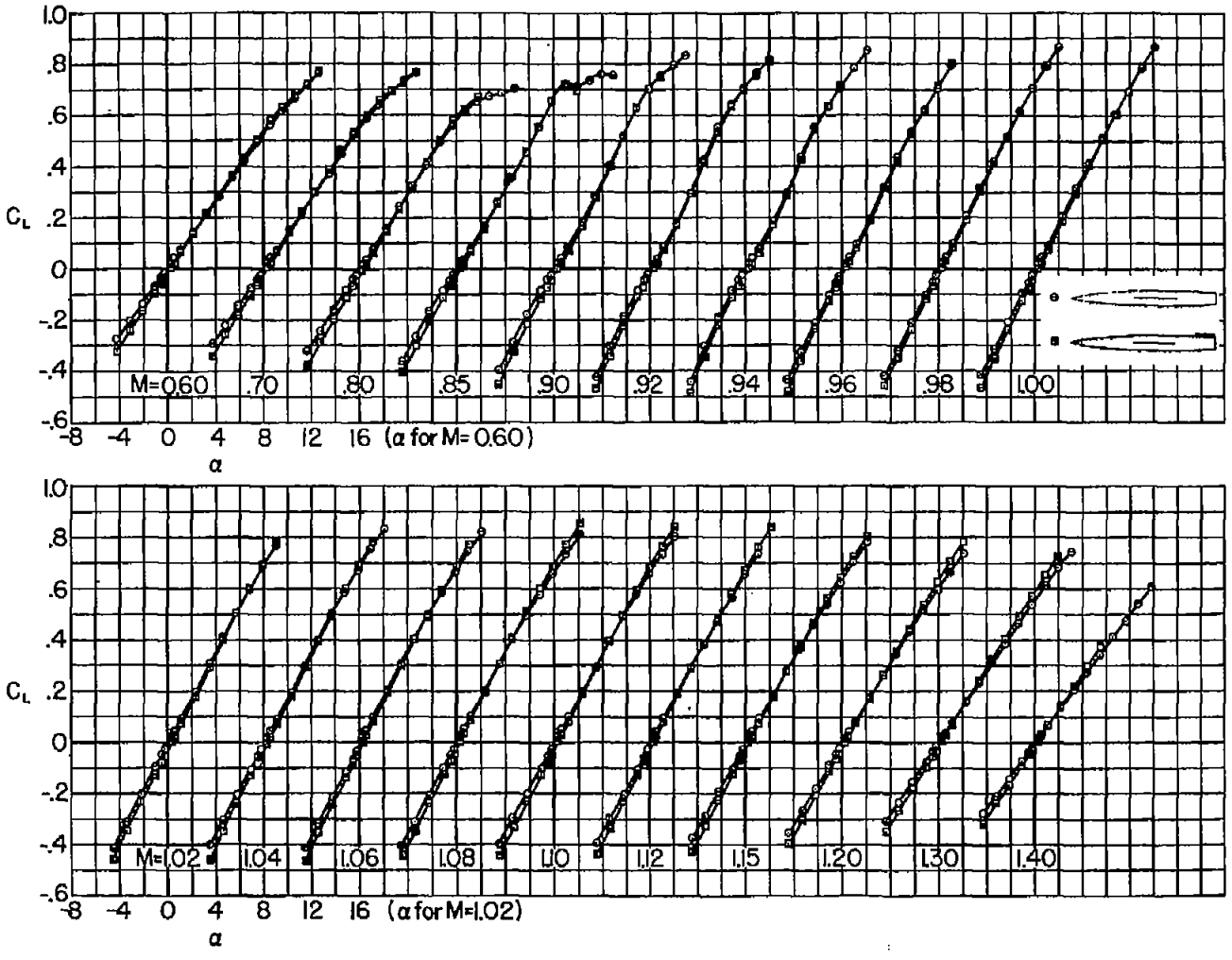

(b) Mid-wing, moderately high tail configuration.

Figure 4.- Continued.

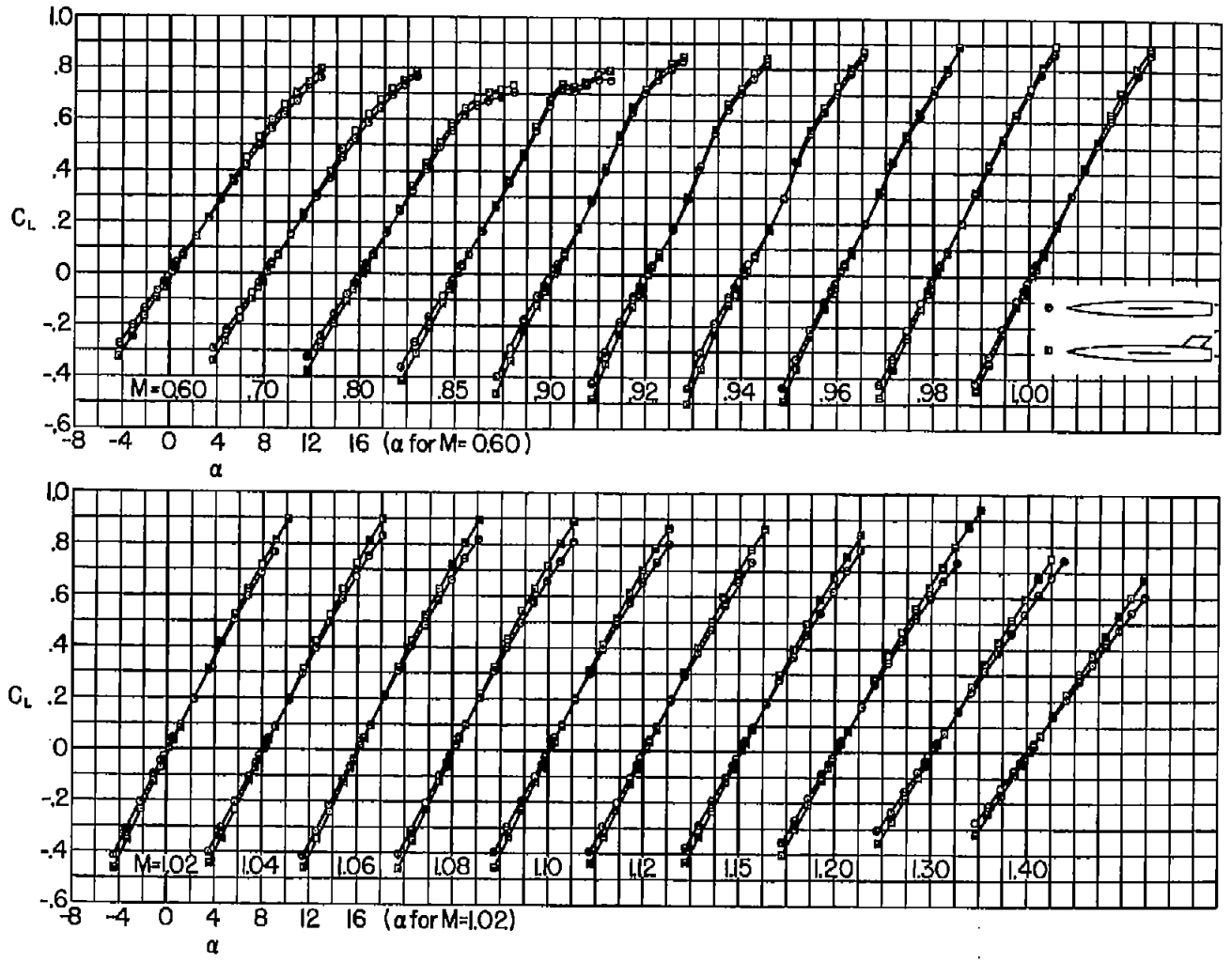

(c) Mid-wing, high-tail configuration.

Figure 4.- Continued.

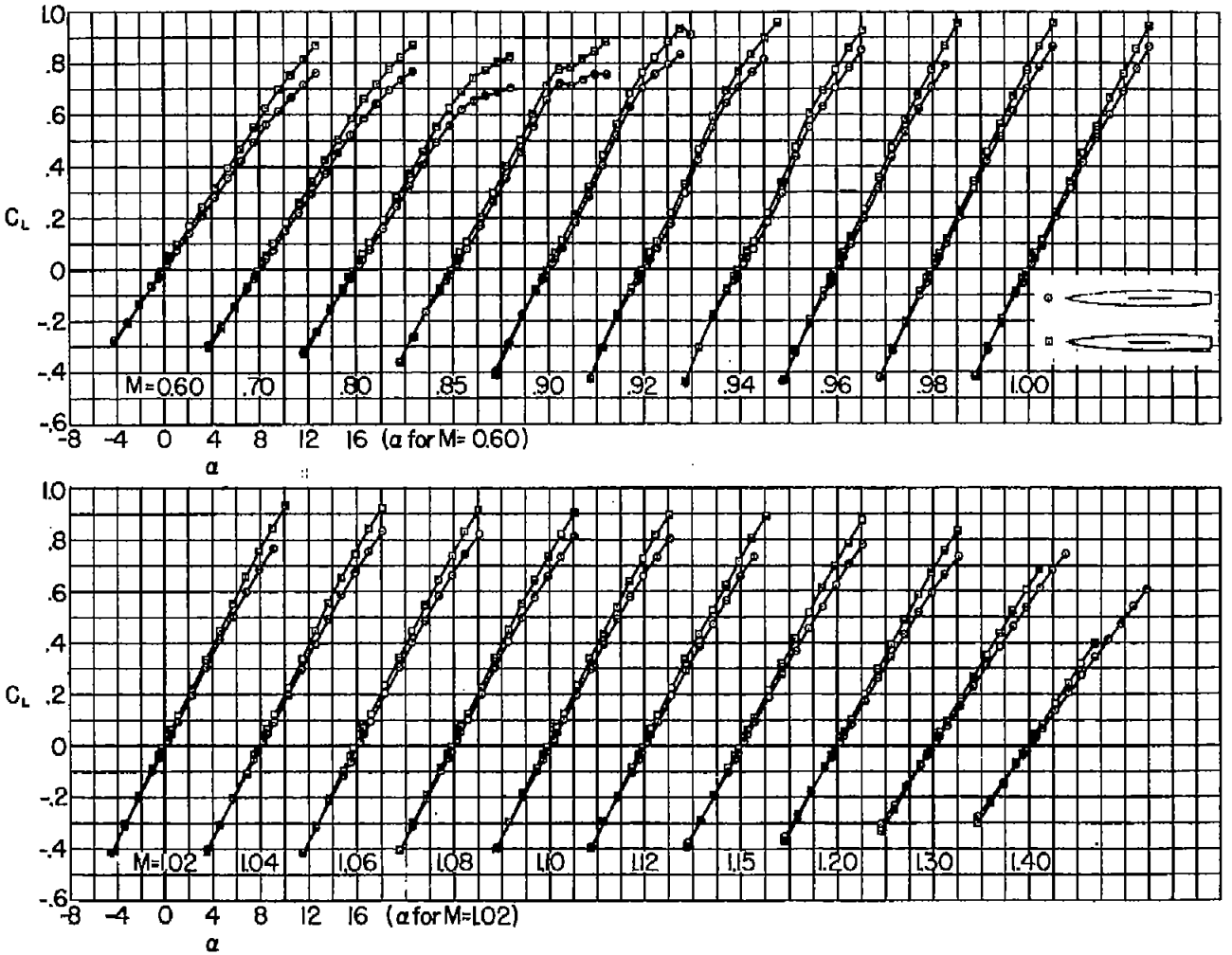

(d) Mid-wing, moderately low tail configuration.

Figure 4.- Continued.

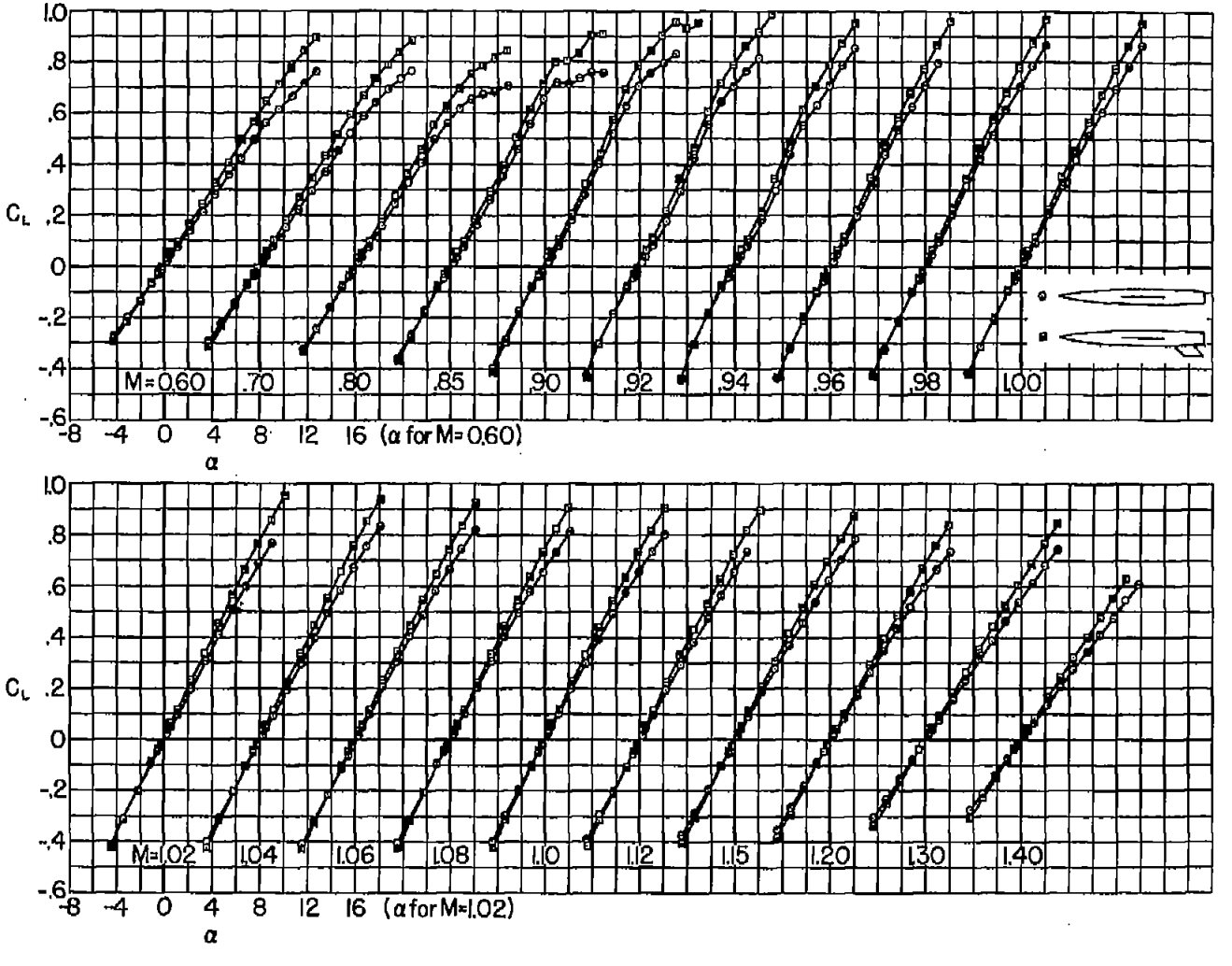

(e) Mid-wing, low-tail configuration.

Figure 4.- Continued.

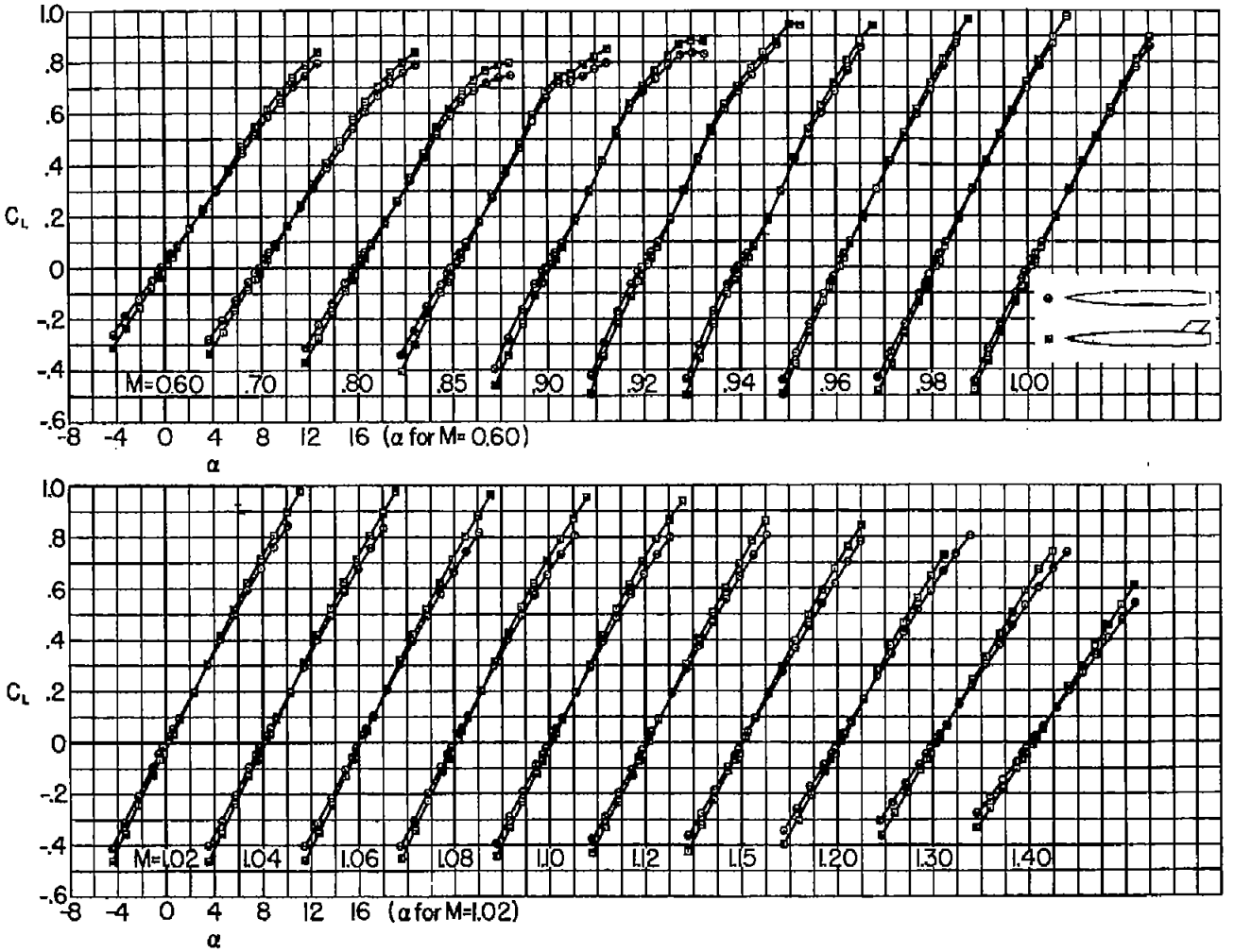

(f) Low-wing, high-tail configuration.

Figure 4.- Continued.

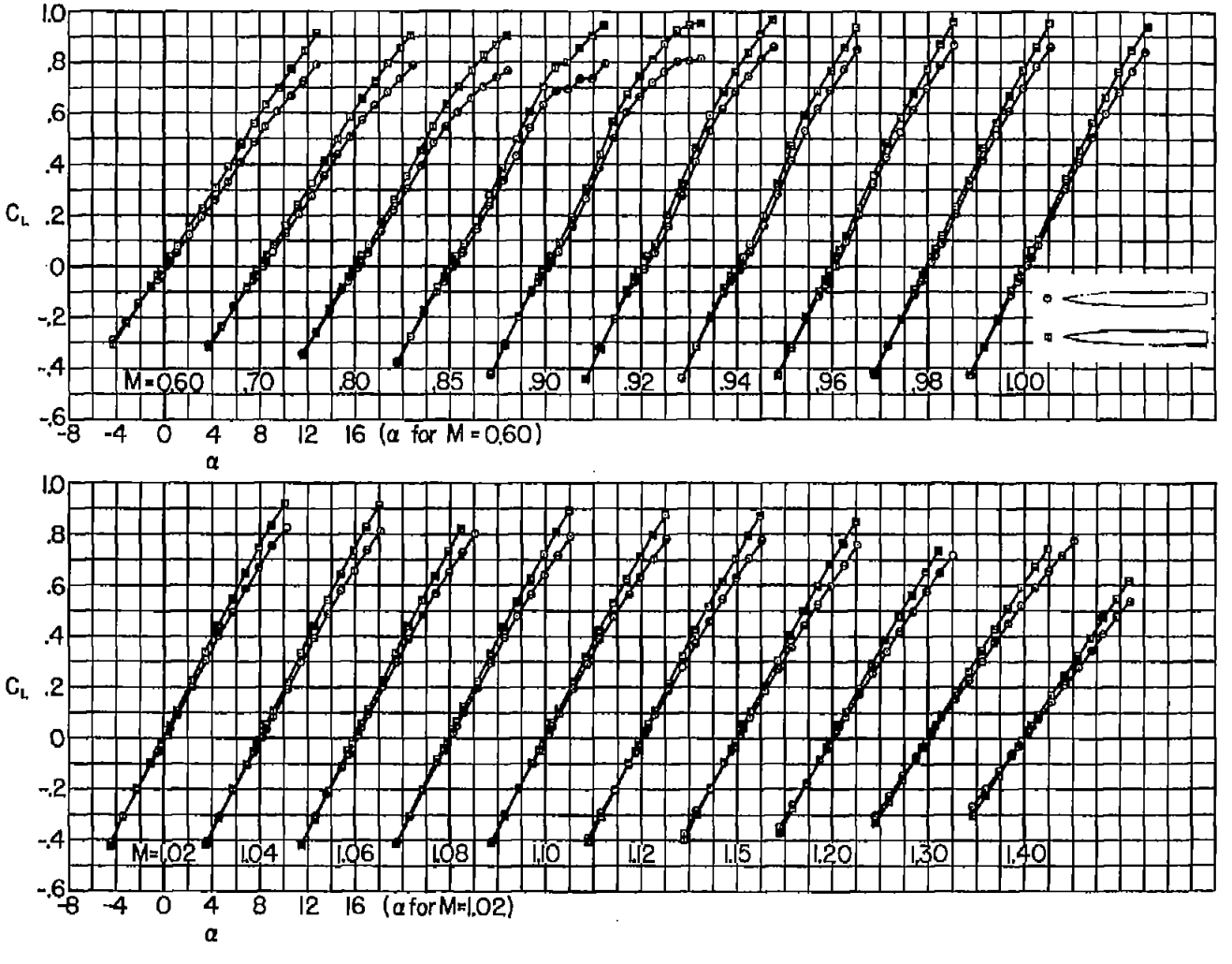

(g) High-wing, moderately low tail configuration.

Figure 4.- Concluded.

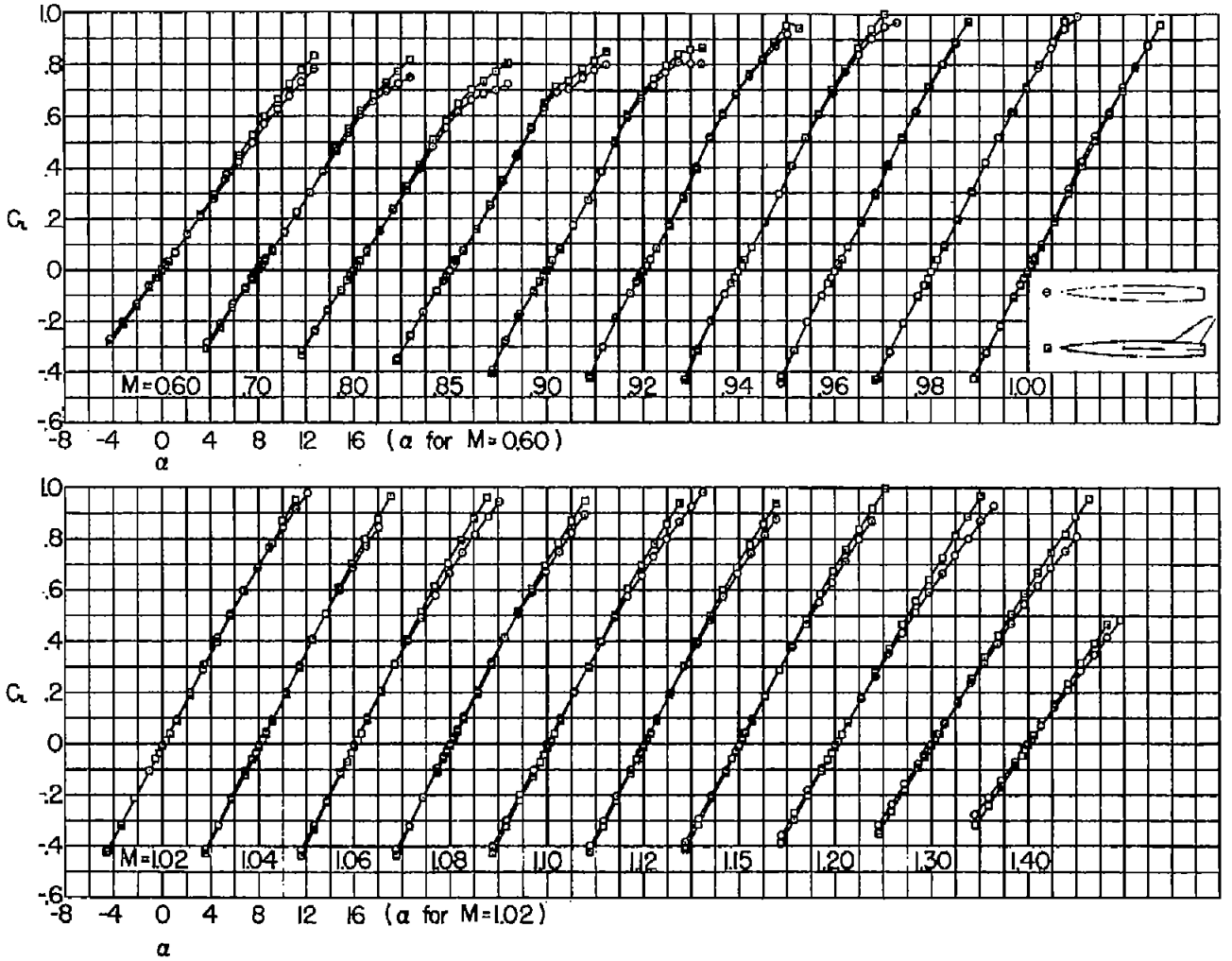

(a) Mid-wing, mid-tail configuration.

Figure 5.- Variation of lift coefficient with angle of attack for constant Mach number; boundary-layer transition fixed.

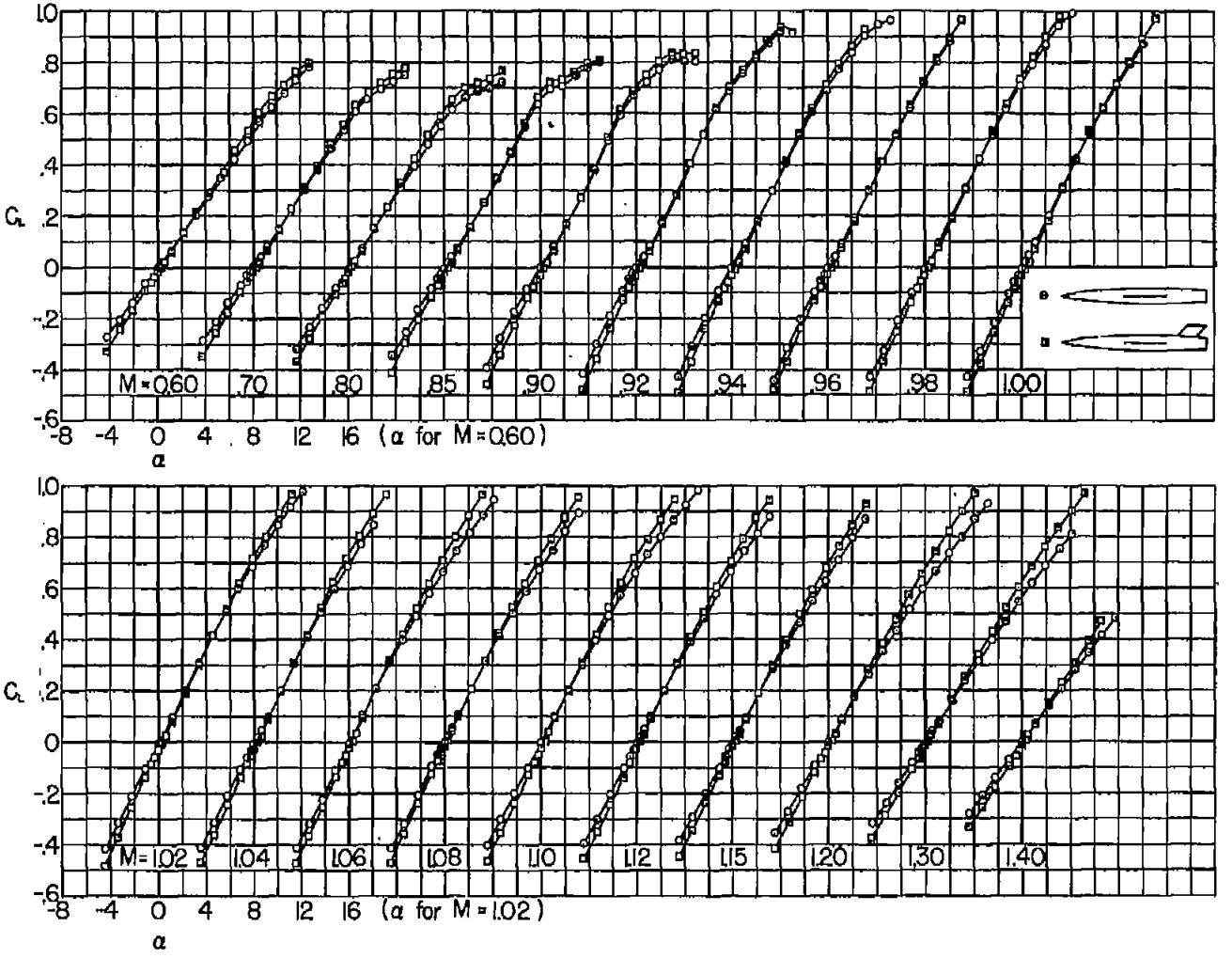

(b) Mid-wing, high-tail configuration.

Figure 5.- Continued.

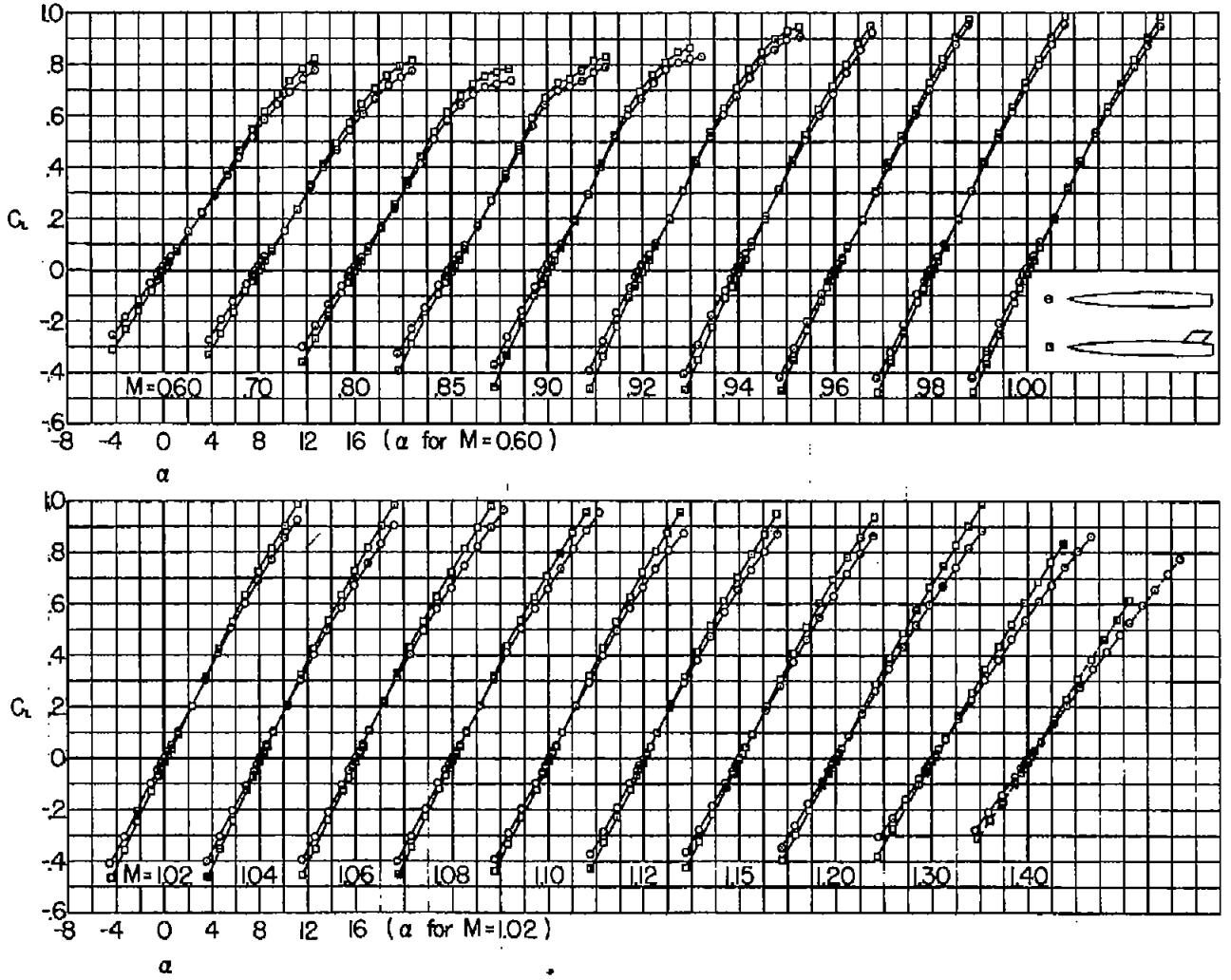

(c) Low-wing, high-tail configuration.

Figure 5.- Concluded.

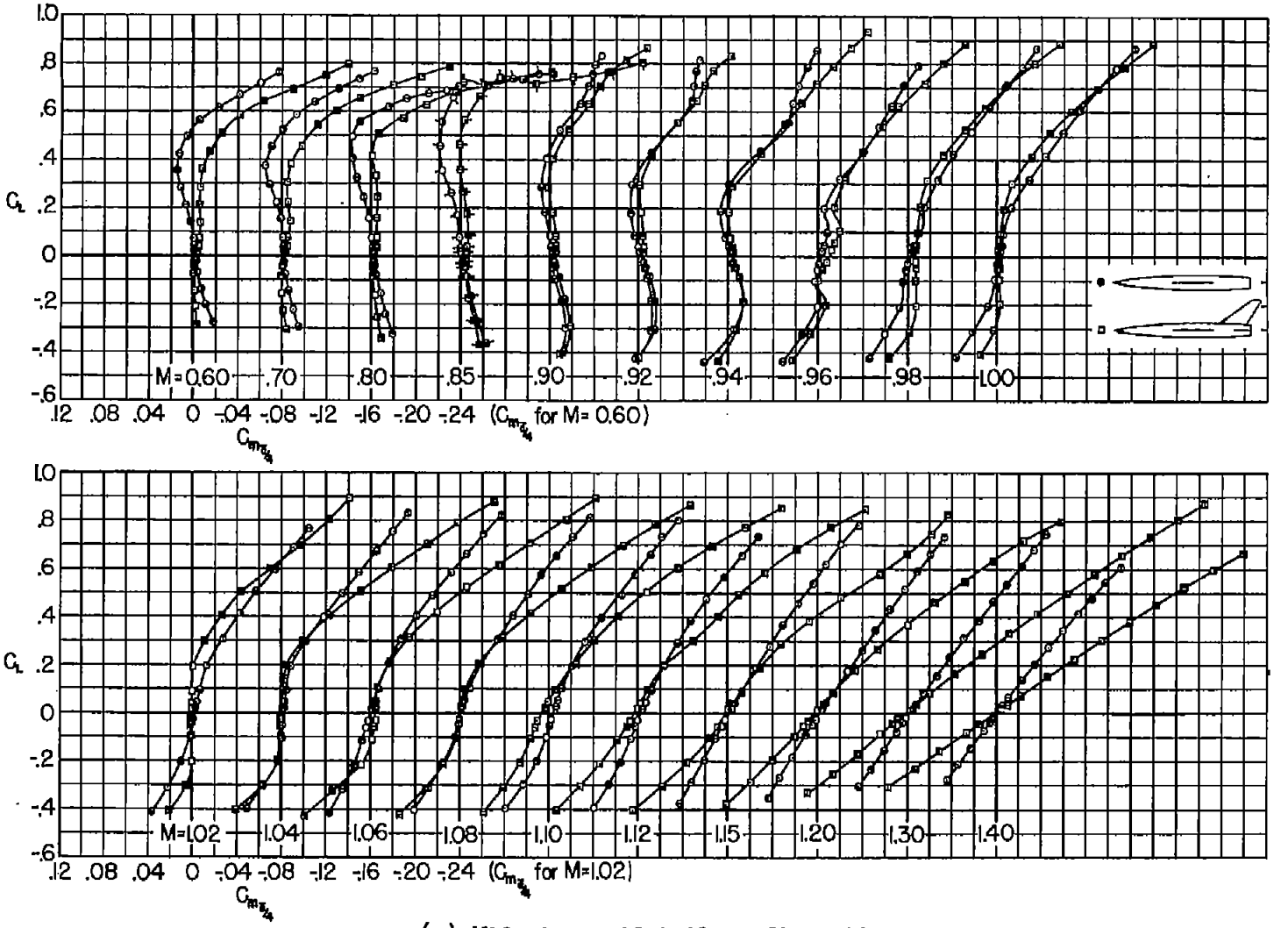

(a) Mid-wing, mid-tail configuration.

Figure 6.- Variation of pitching-moment coefficient with lift coefficient for constant Mach number; boundary-layer transition free.

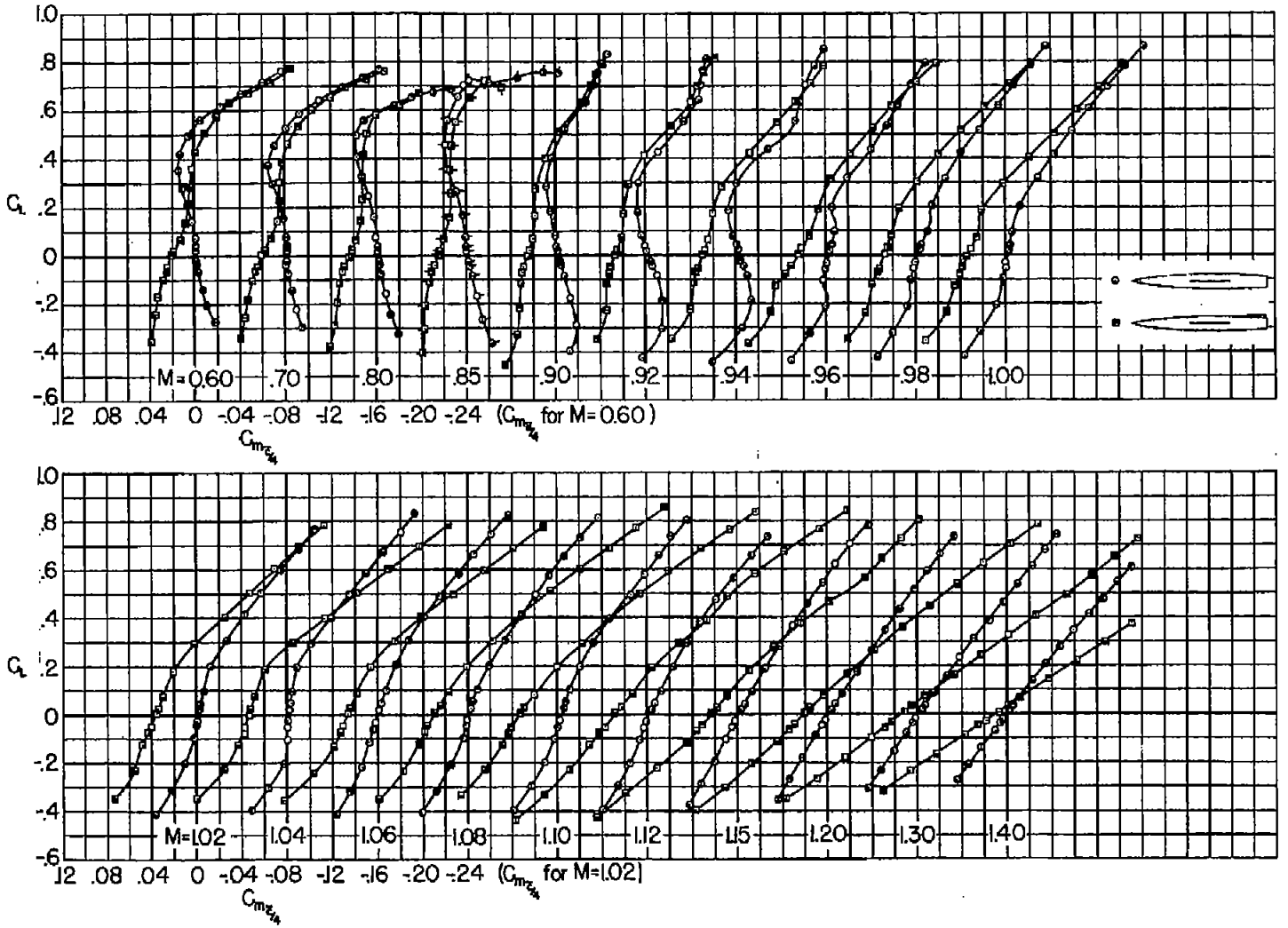

(b) Mid-wing, moderately high tail configuration.

Figure 6.- Continued.

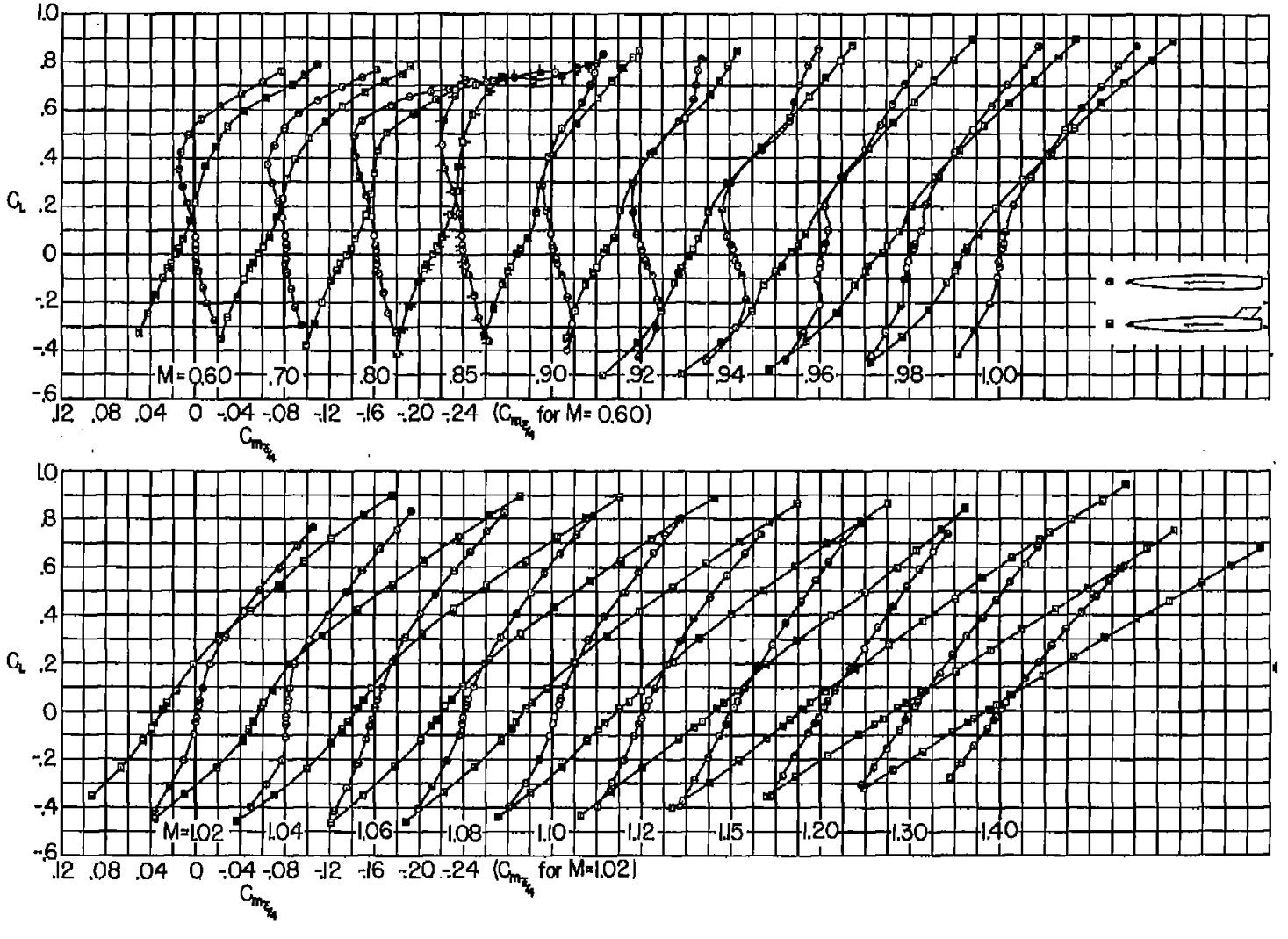

(c) Mid-wing, high-tail configuration.

Figure 6.- Continued.

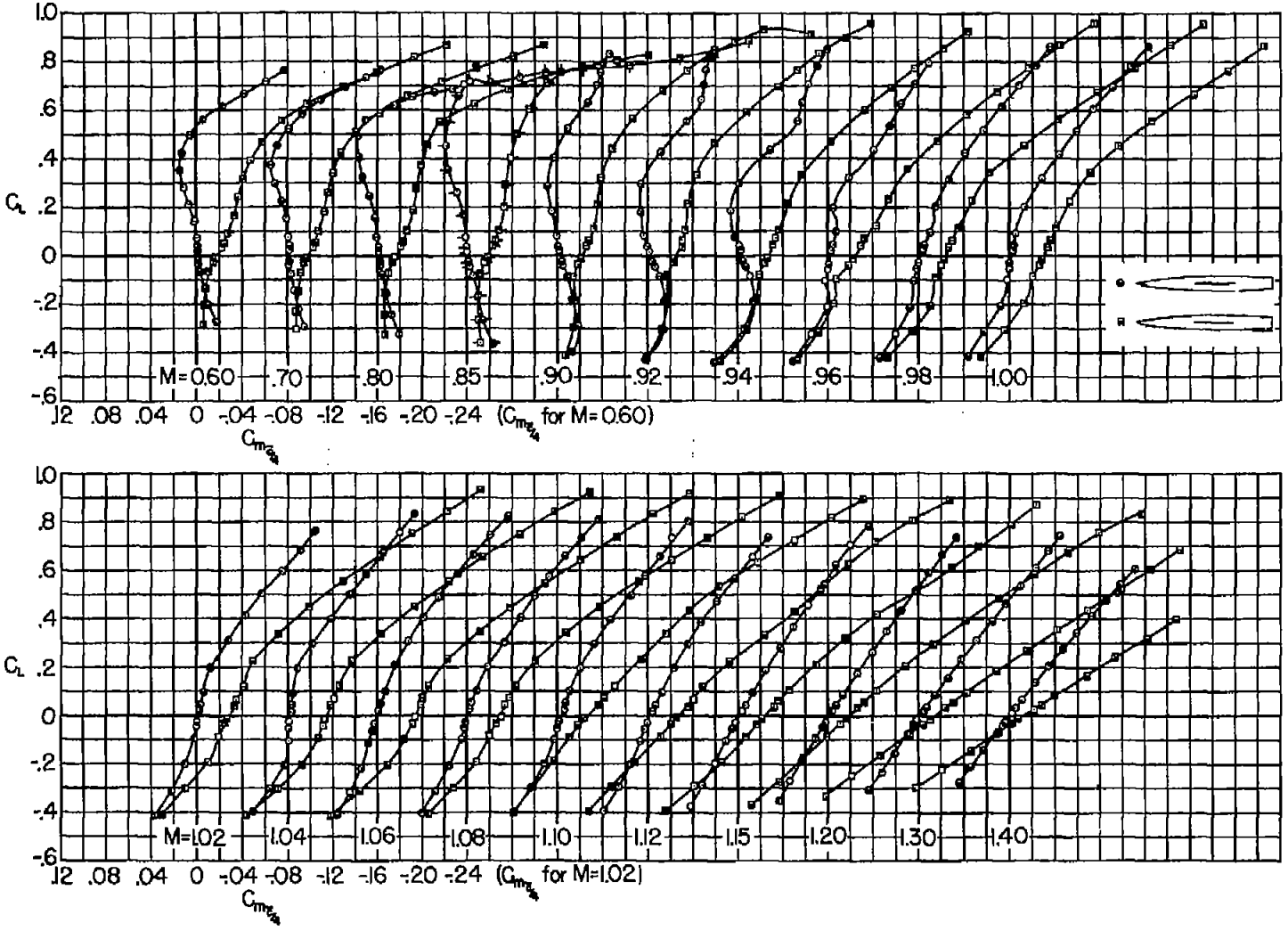

(d) Mid-wing, moderately low tail configuration.

Figure 6.- Continued.

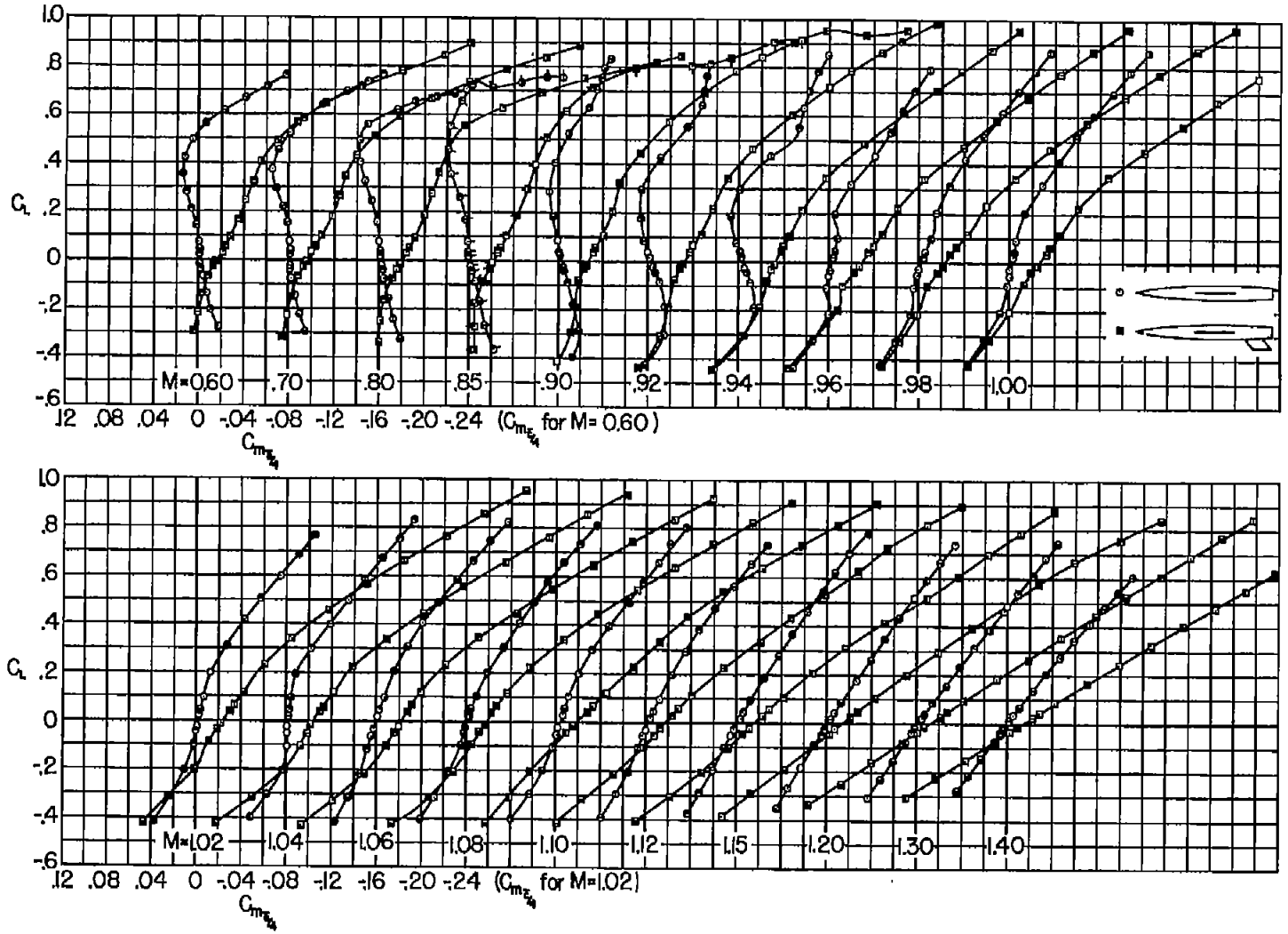

(e) Mid-wing, low-tail configuration.

Figure 6.- Continued.

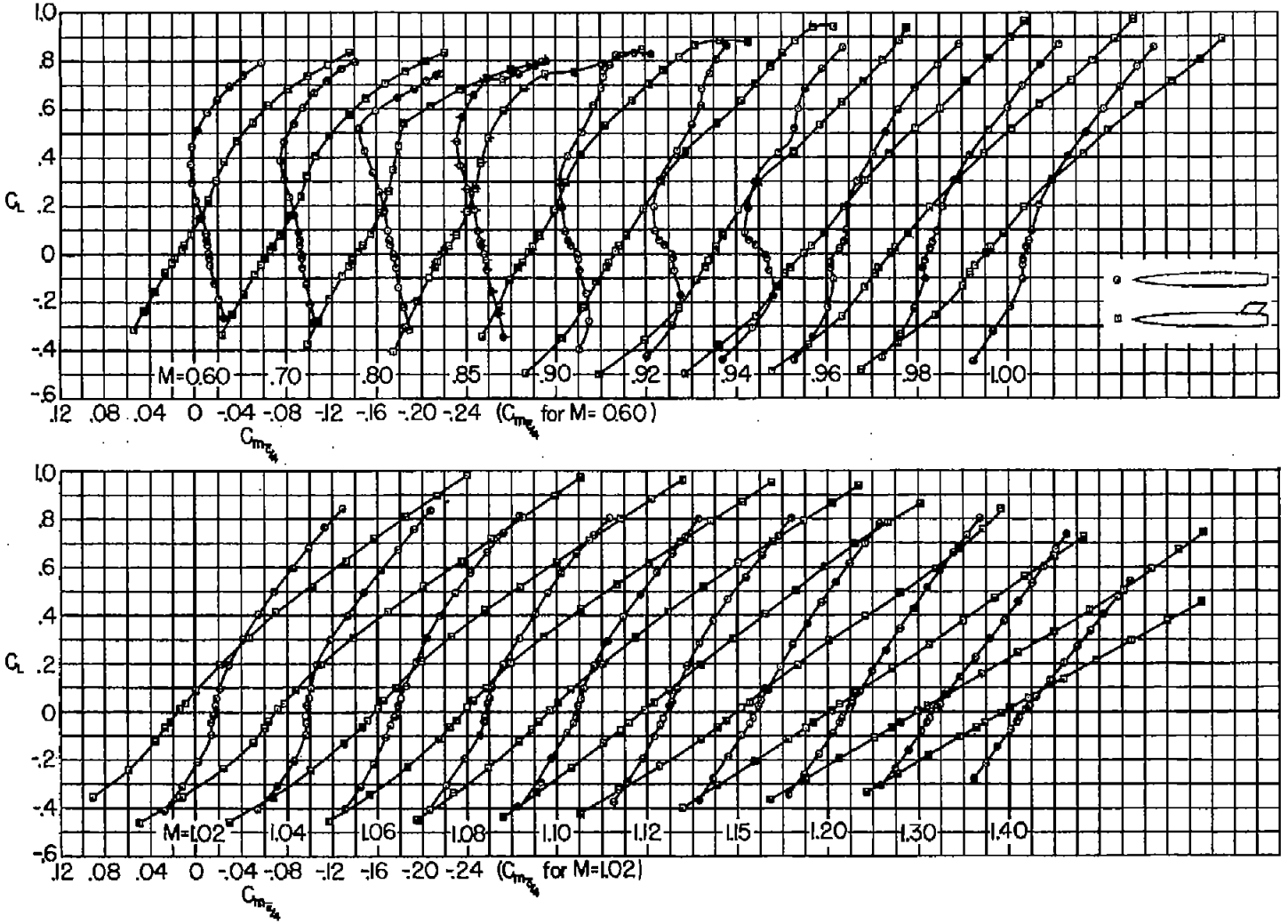

(f) Low-wing, high-tail configuration.

Figure 6.- Continued.

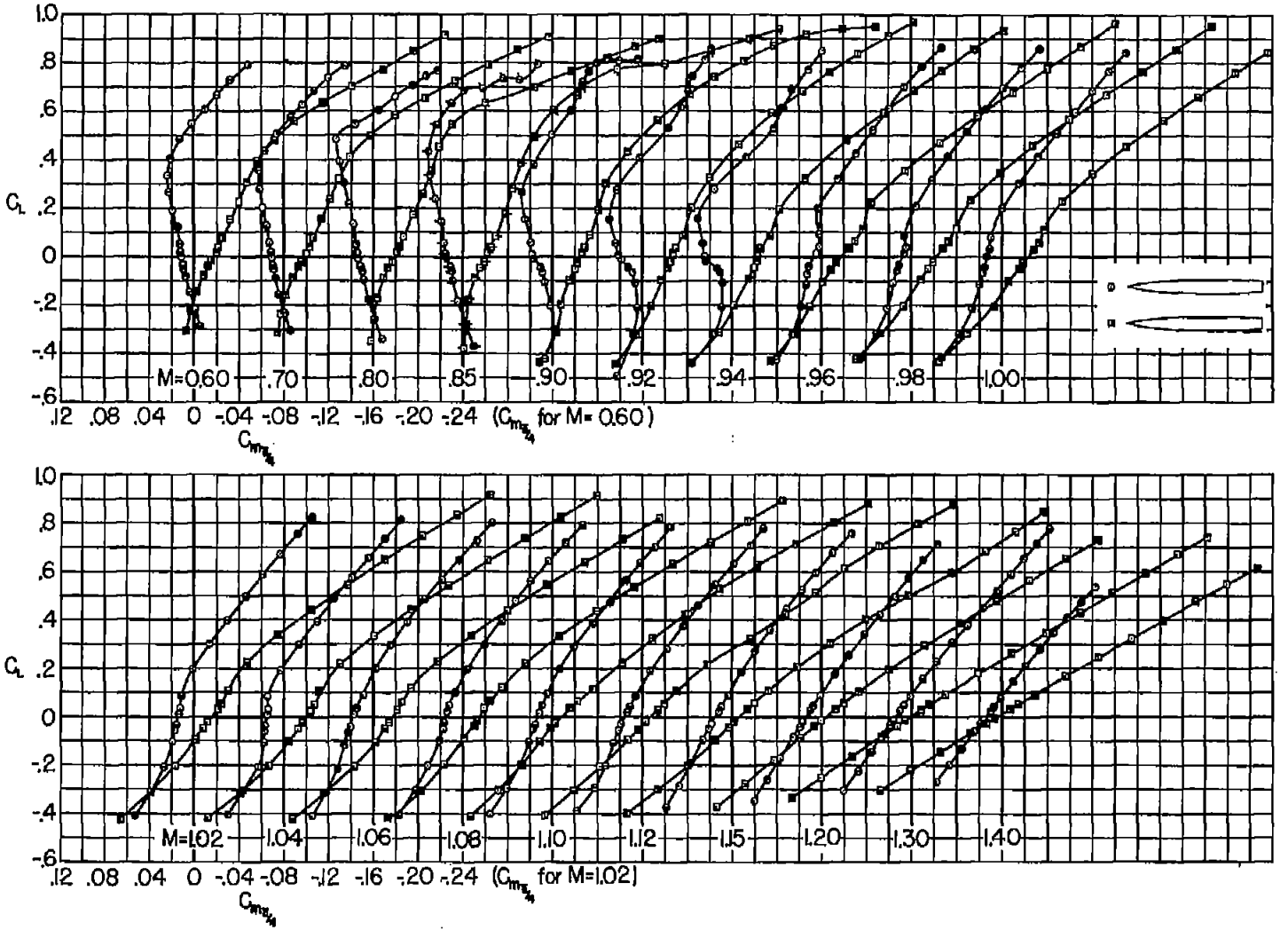

(g) High-wing, moderately low tail configuration.

Figure 6.- Concluded.

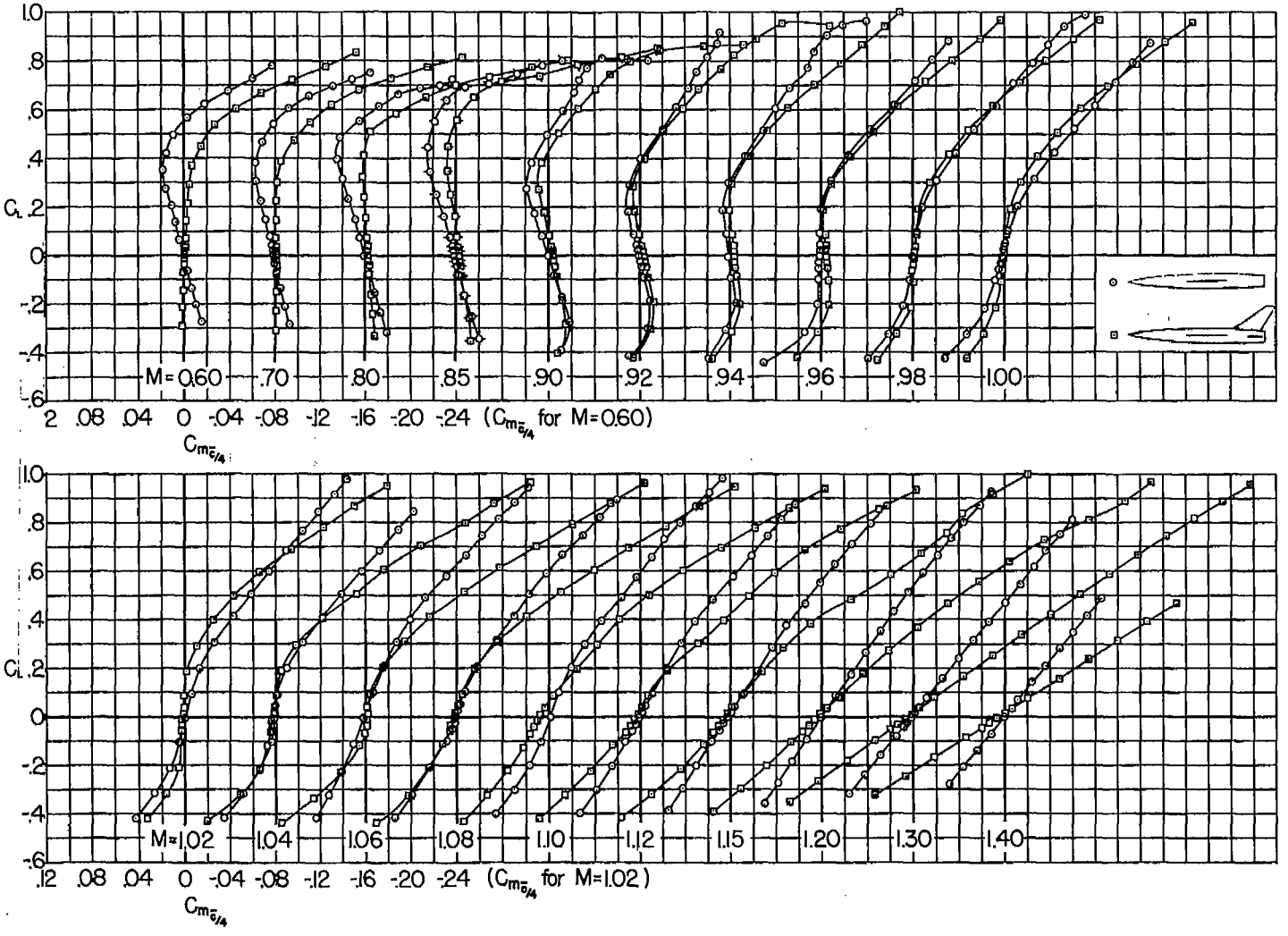

(a) Mid-wing, mid-tail configuration.

Figure 7.- Variation of pitching-moment coefficient with lift coefficient for constant Mach number; boundary-layer transition fixed.

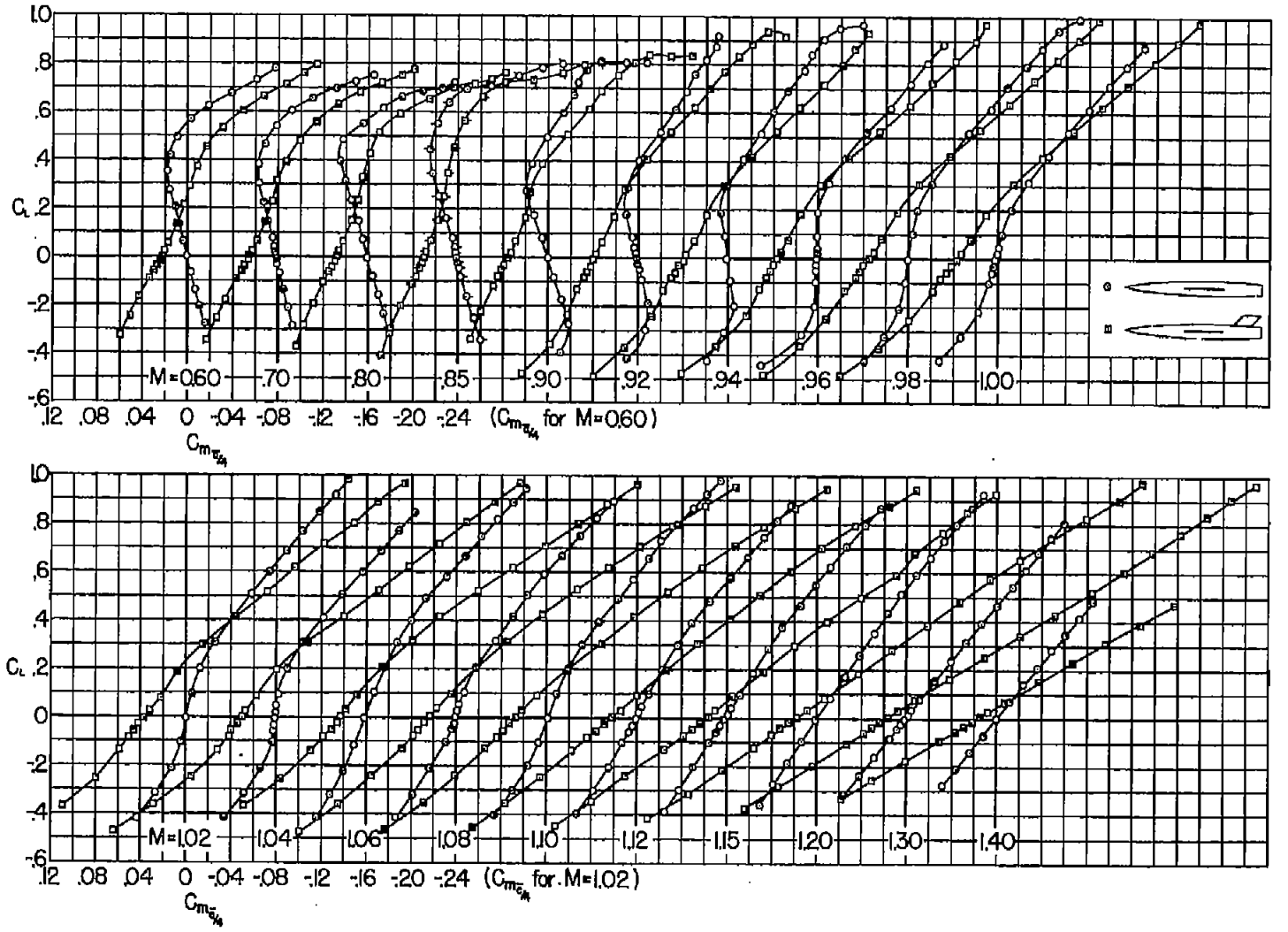

(b) Mid-wing, high-tail configuration.

Figure 7.- Continued.

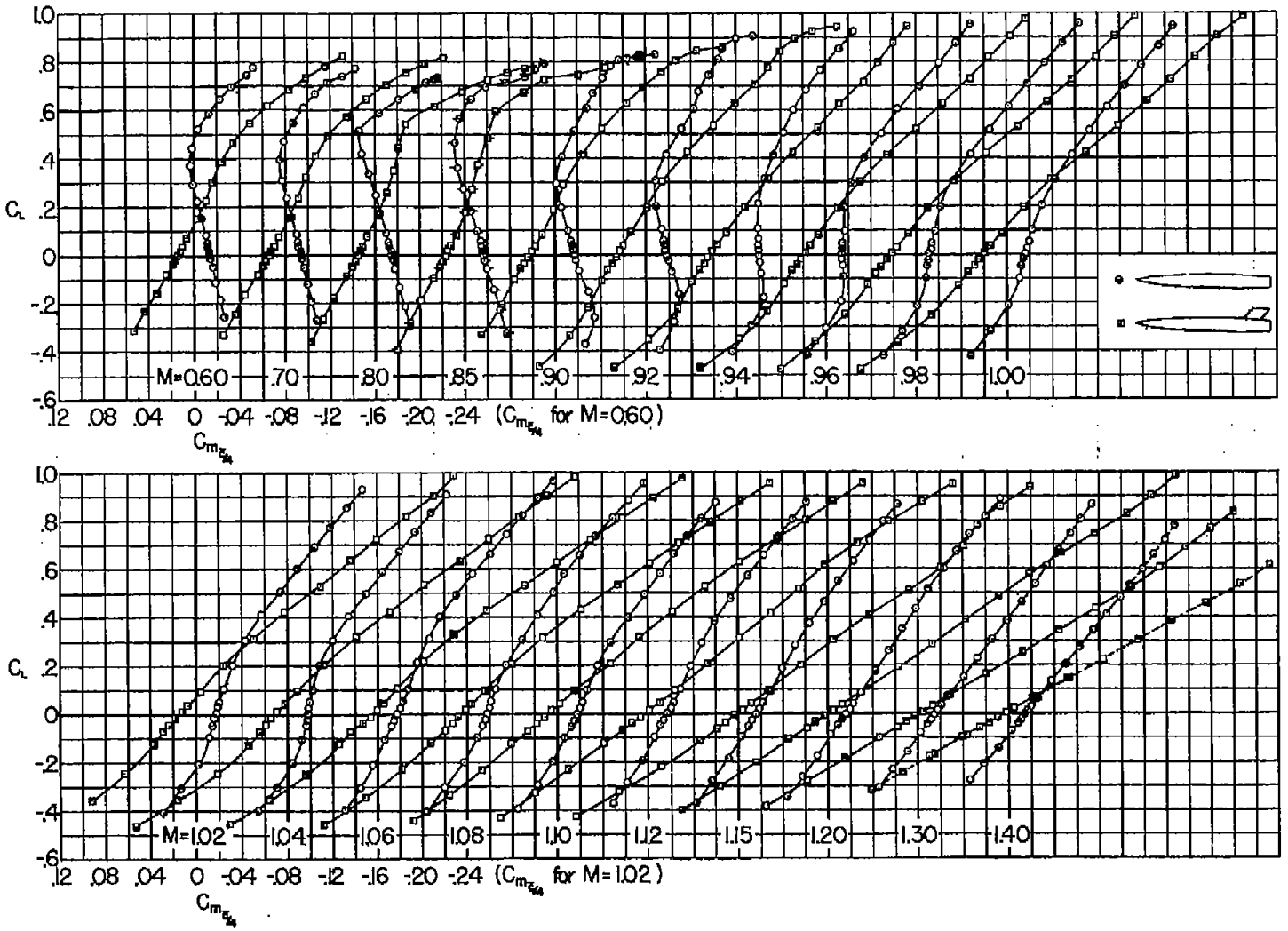

(c) Low-wing, high-tail configuration.

Figure 7.- Concluded.

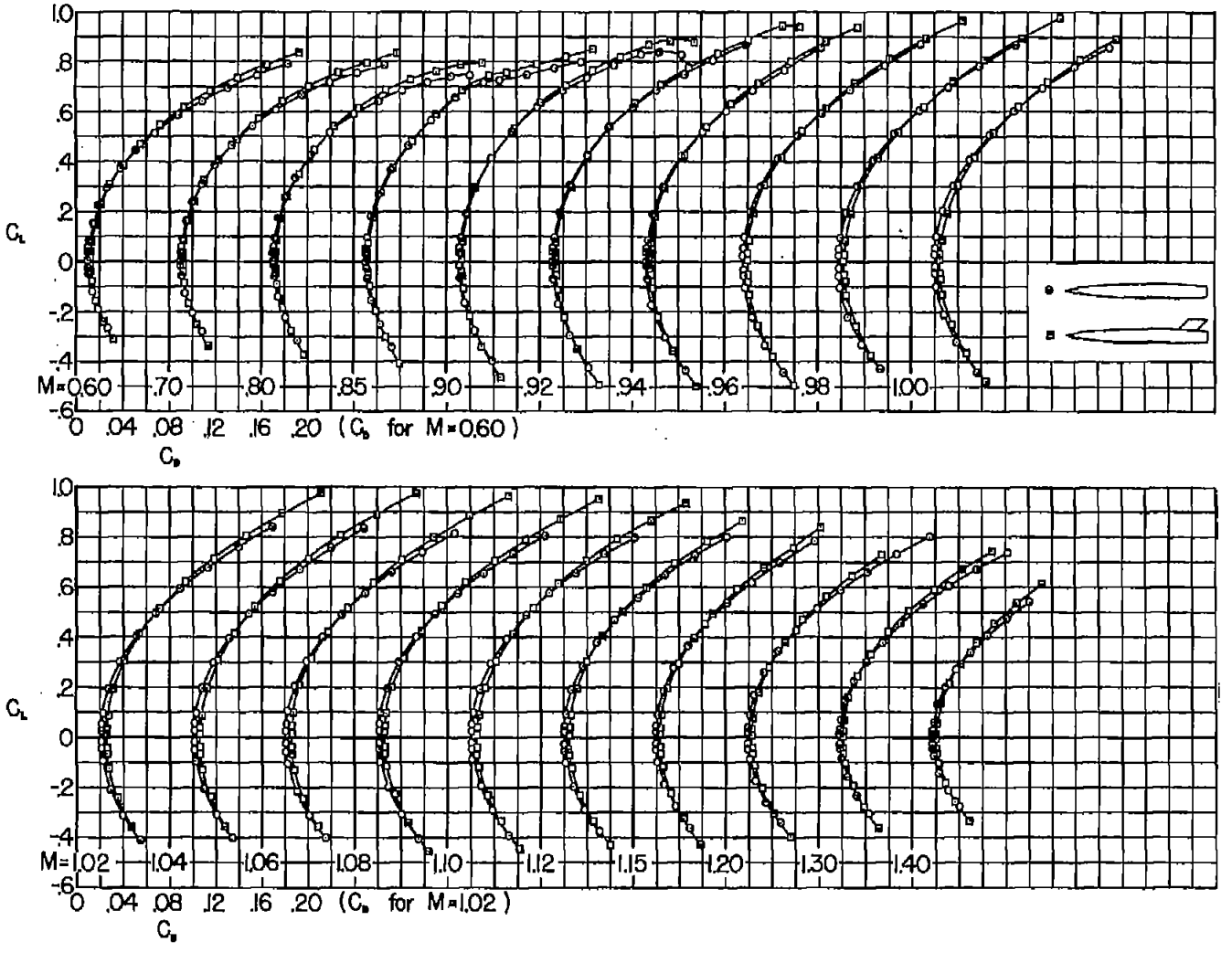

(a) Low-wing, high-tail configuration.

Figure 8.- Variation of drag coefficient with lift coefficient for constant Mach number; boundary-layer transition free.

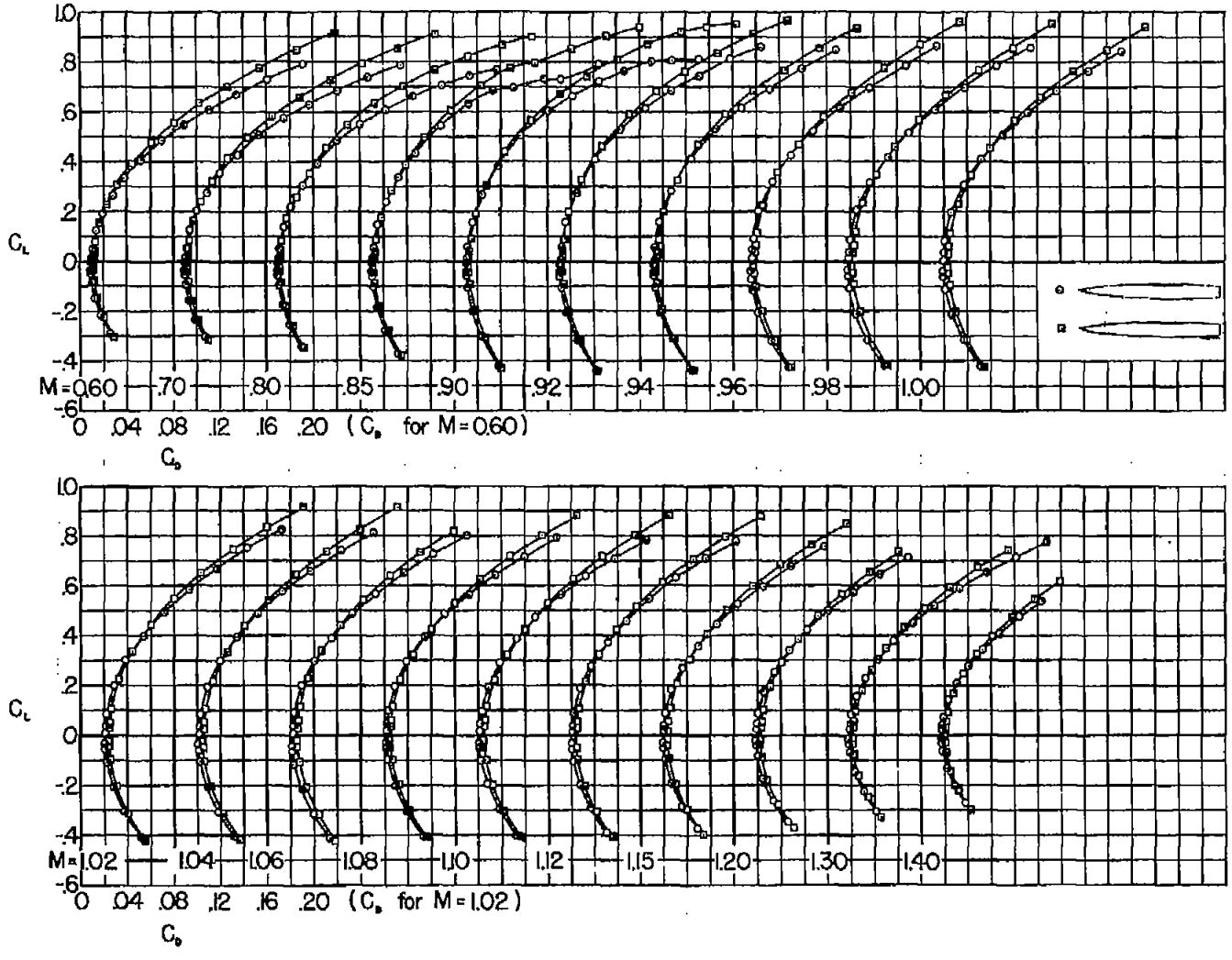

(b) High-wing, moderately low tail configuration.

Figure 8.- Concluded.

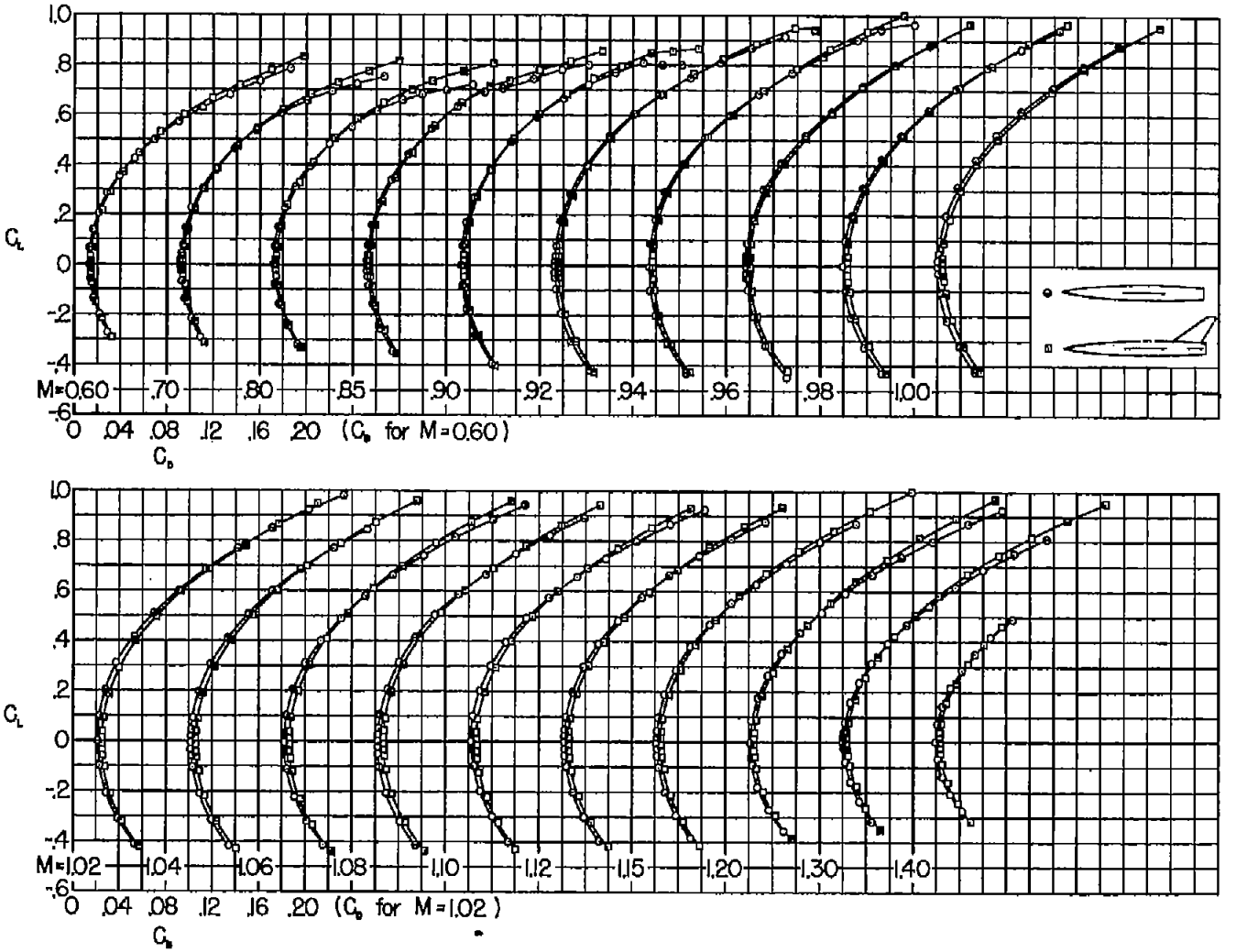

(a) Mid-wing, mid-tail configuration.

Figure 9.- Variation of drag coefficient with lift coefficient for constant Mach number; boundary-layer transition fixed.

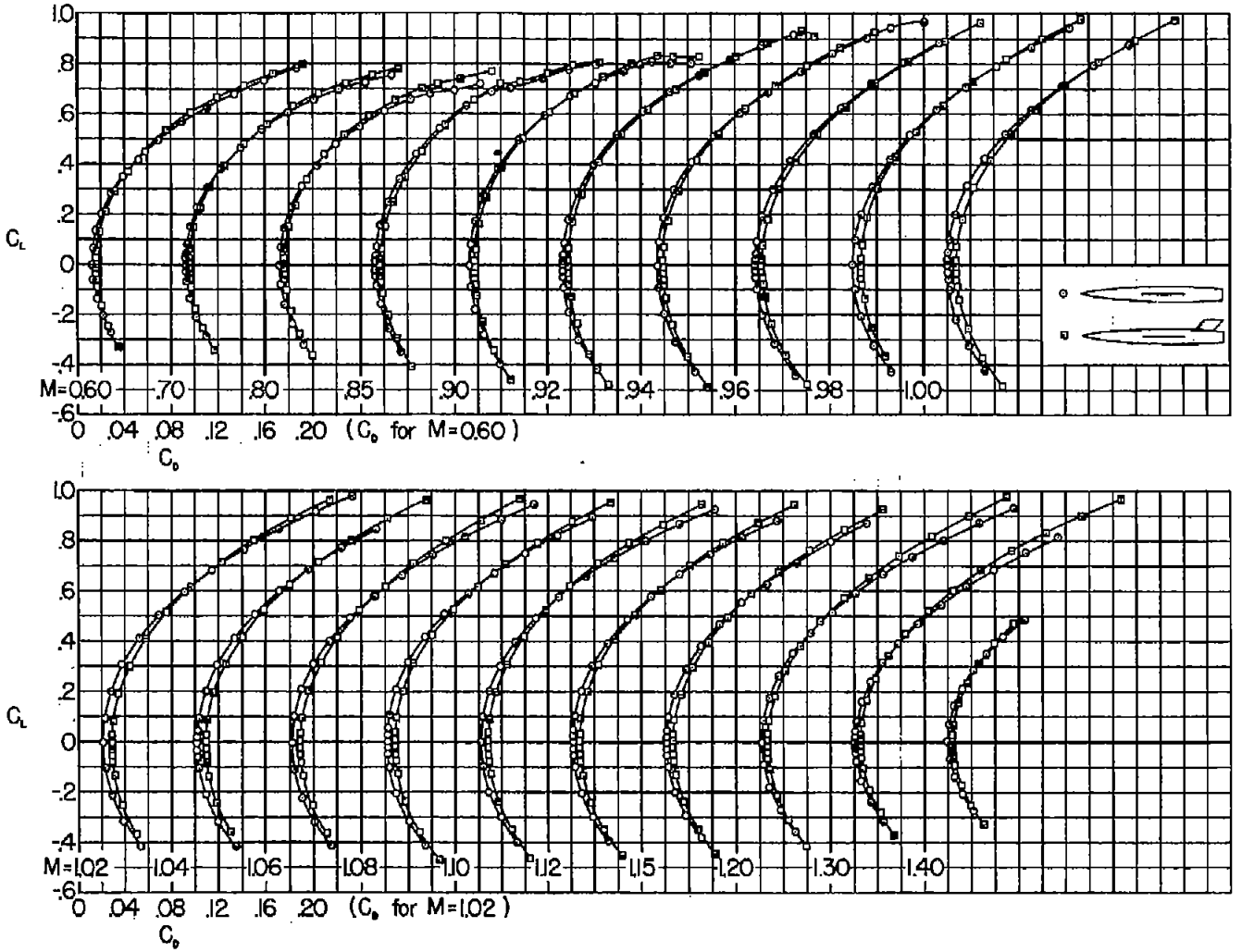

(b) Mid-wing, high-tail configuration.

Figure 9.- Continued.

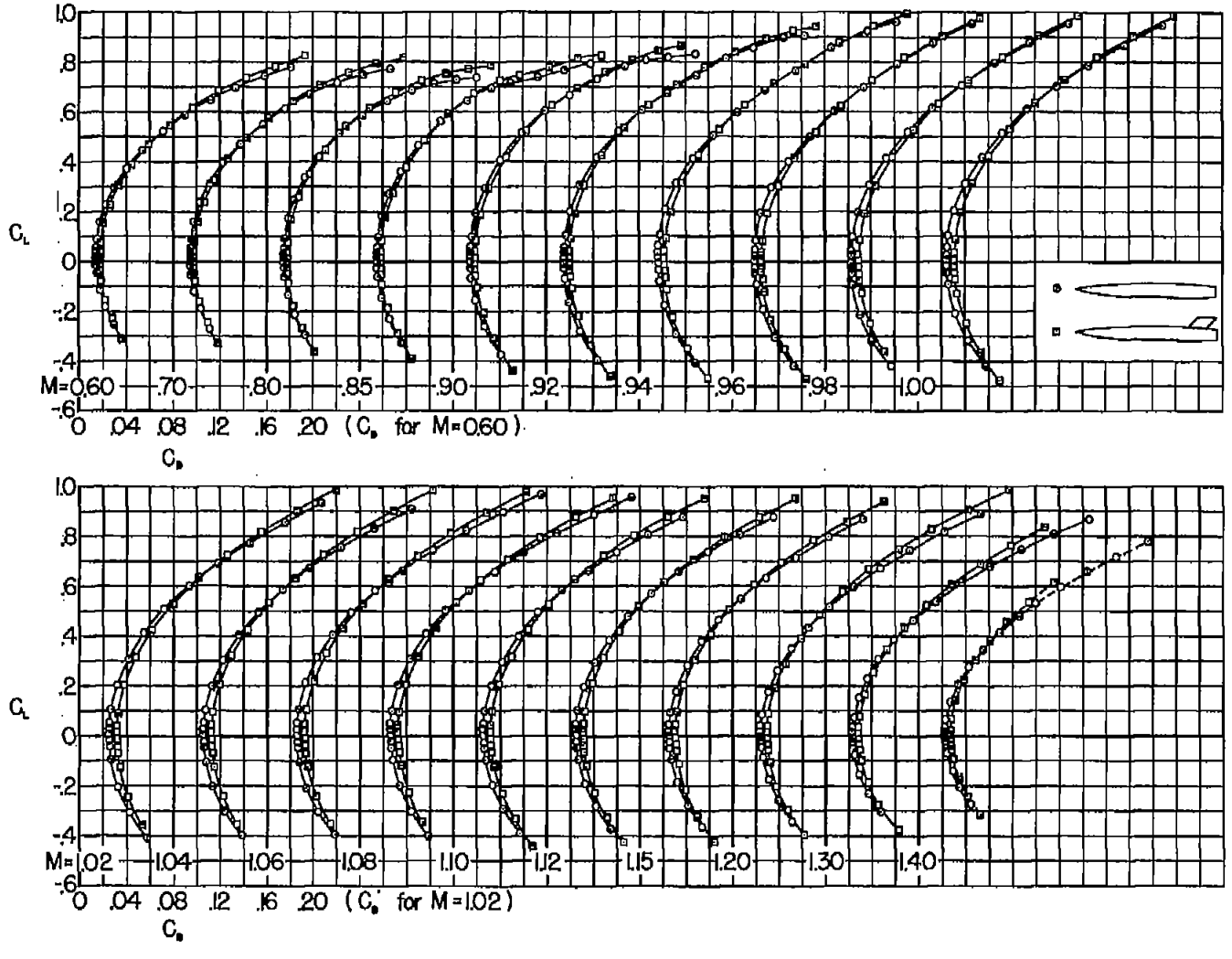

(c) Low-wing, high-tail configuration.

Figure 9.- Concluded.

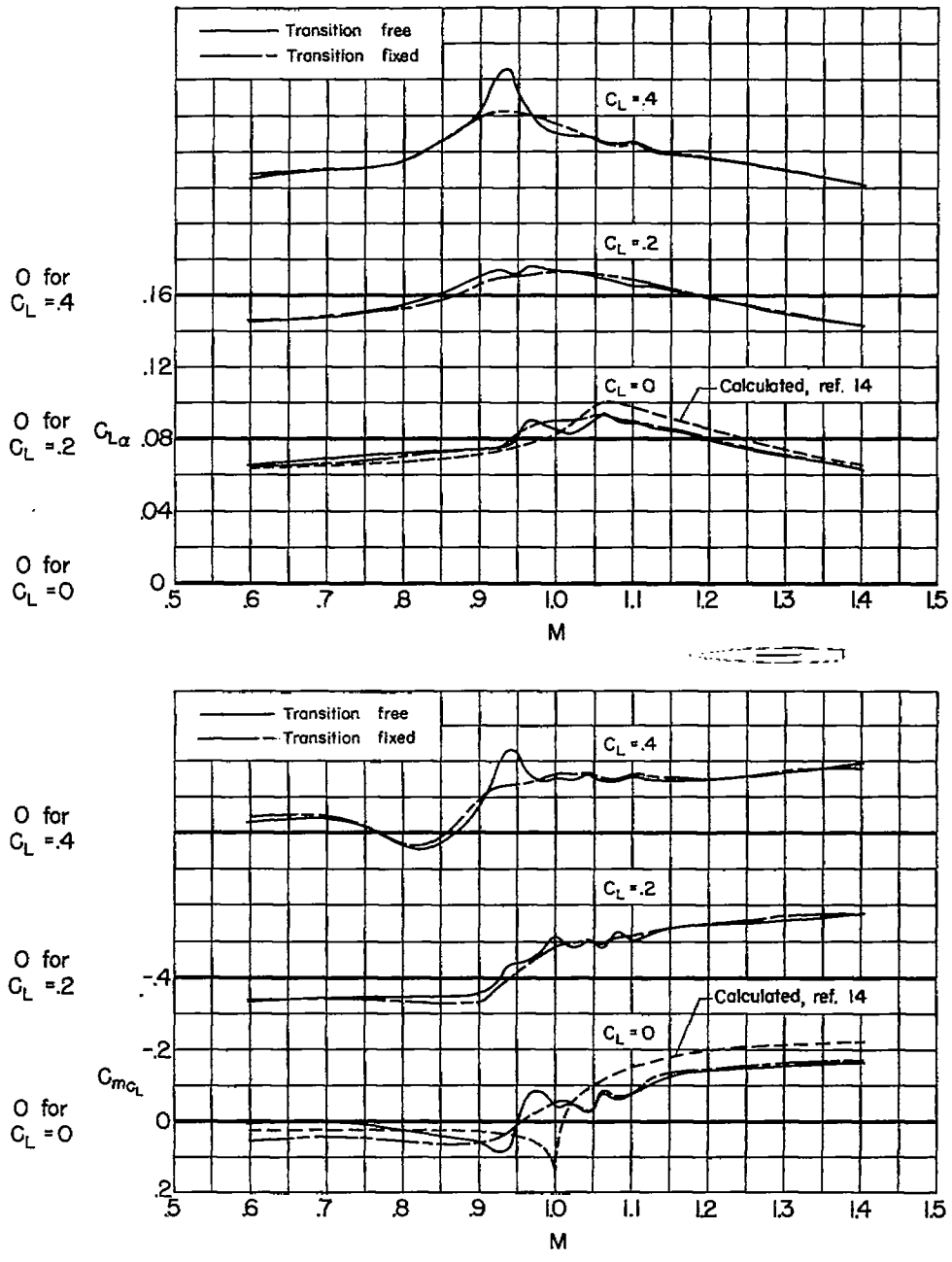

(a) Mid-wing configuration.

Figure 10.- Effect of Mach number on C_{L_α} and $C_{m_{C_L}}$ of the wing-body configurations; boundary-layer transition fixed and free.

[redacted]

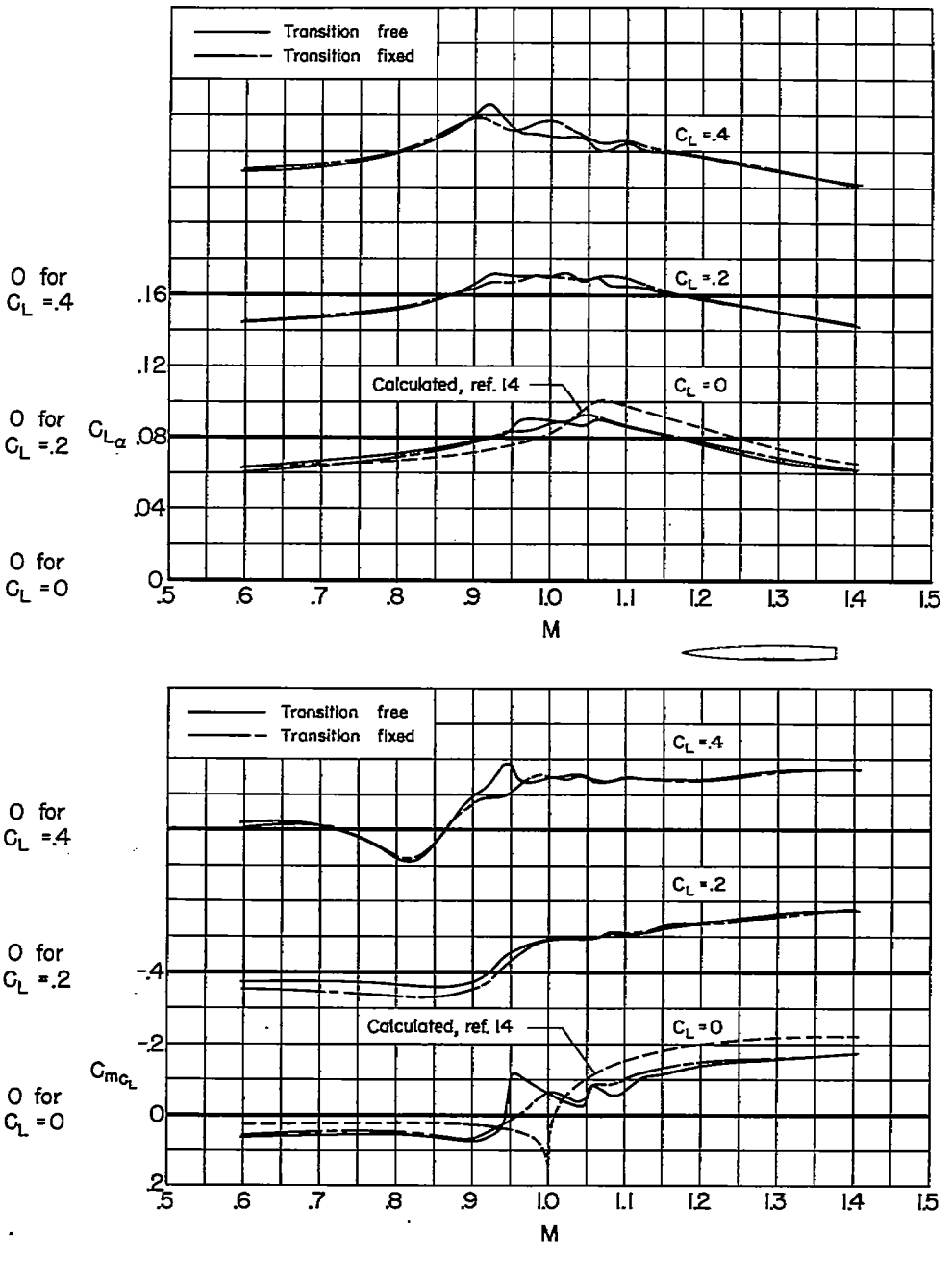

(b) Low-wing configuration.

Figure 10.- Continued.

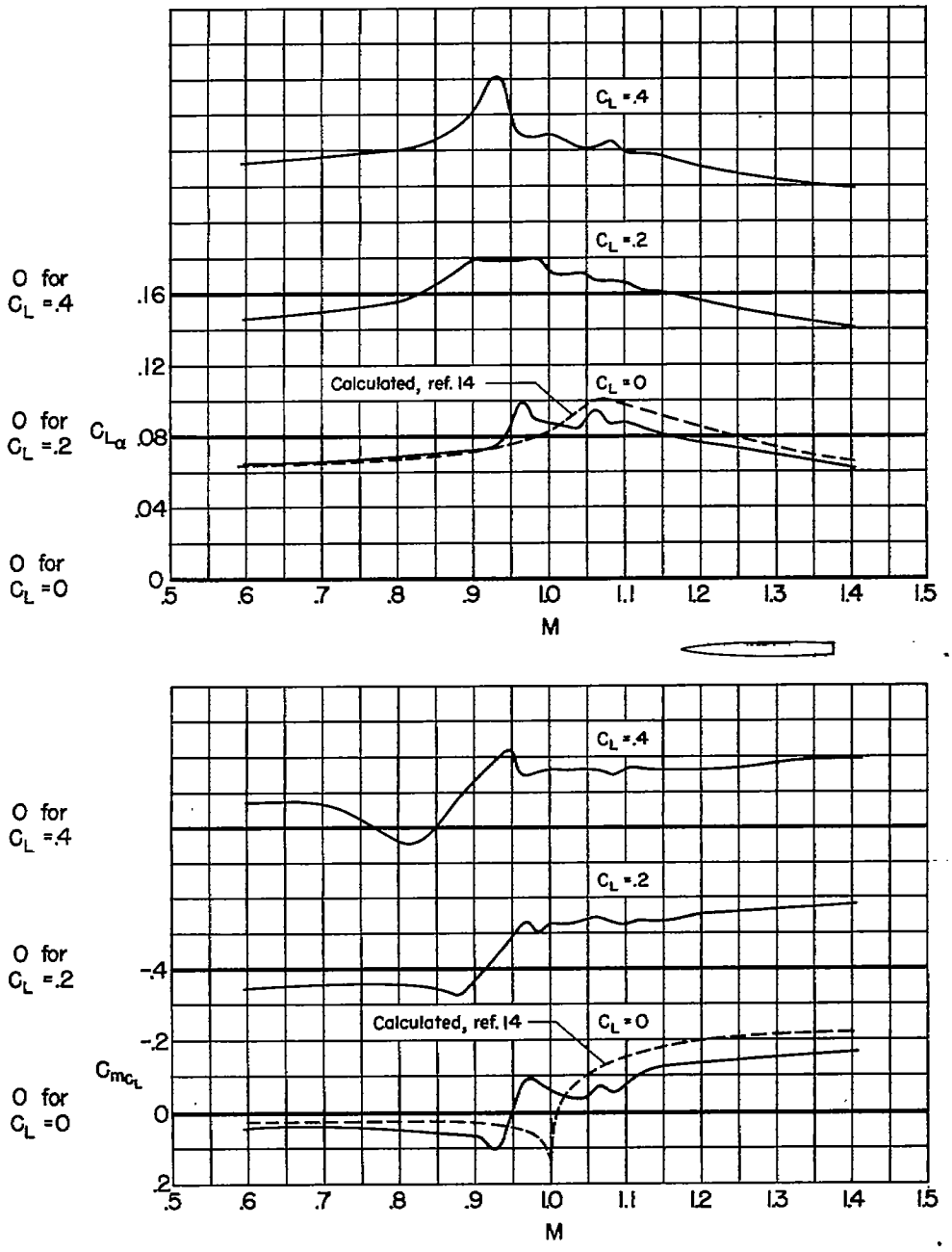

(c) High-wing configuration; transition free.

Figure 10.- Concluded.

[redacted]

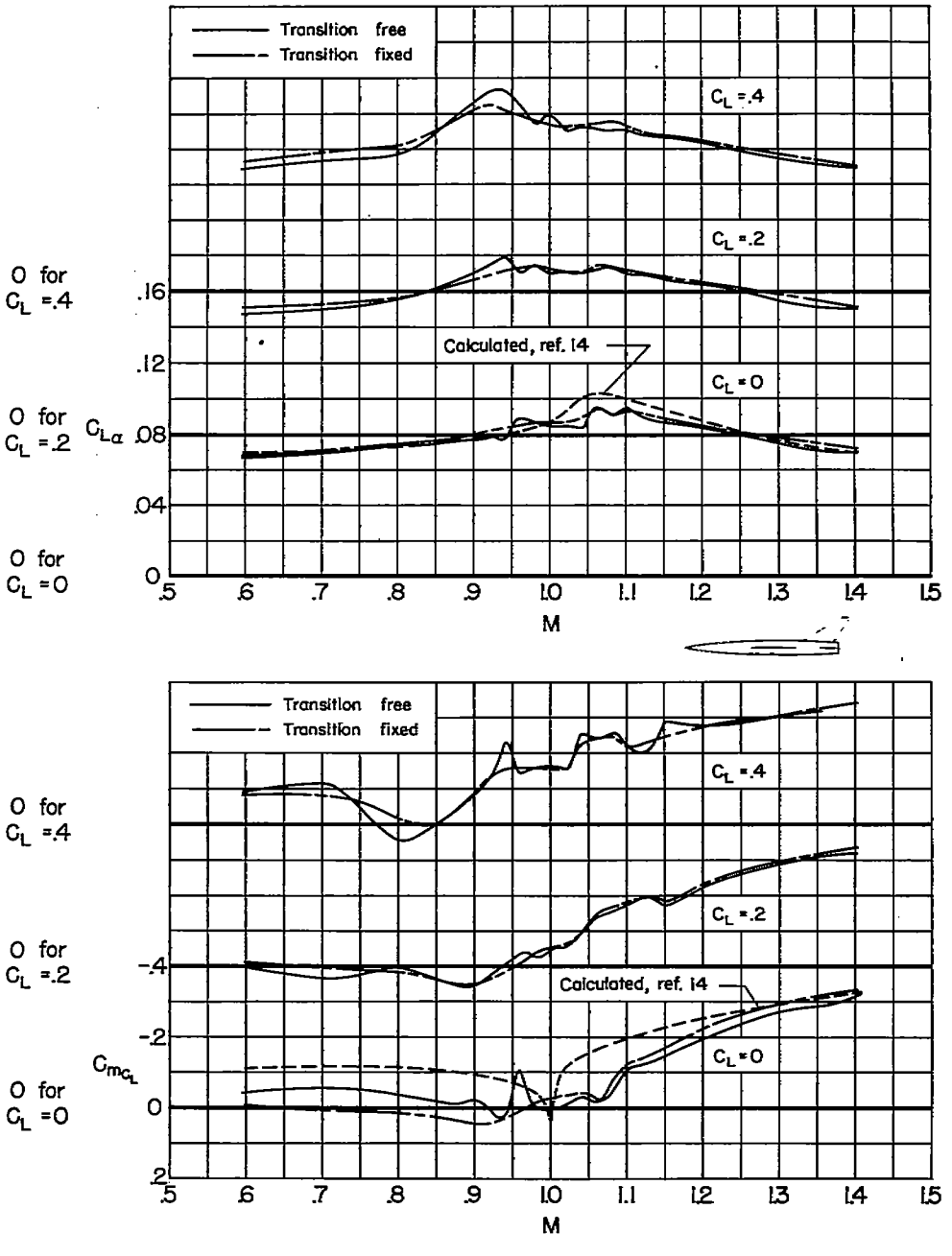

(a) Mid-wing, mid-tail configuration.

Figure 11.- Effect of Mach number on C_{L_α} and $C_{m_{C_L}}$ of the wing-body-tail configurations; boundary-layer transition fixed and free.

[redacted]

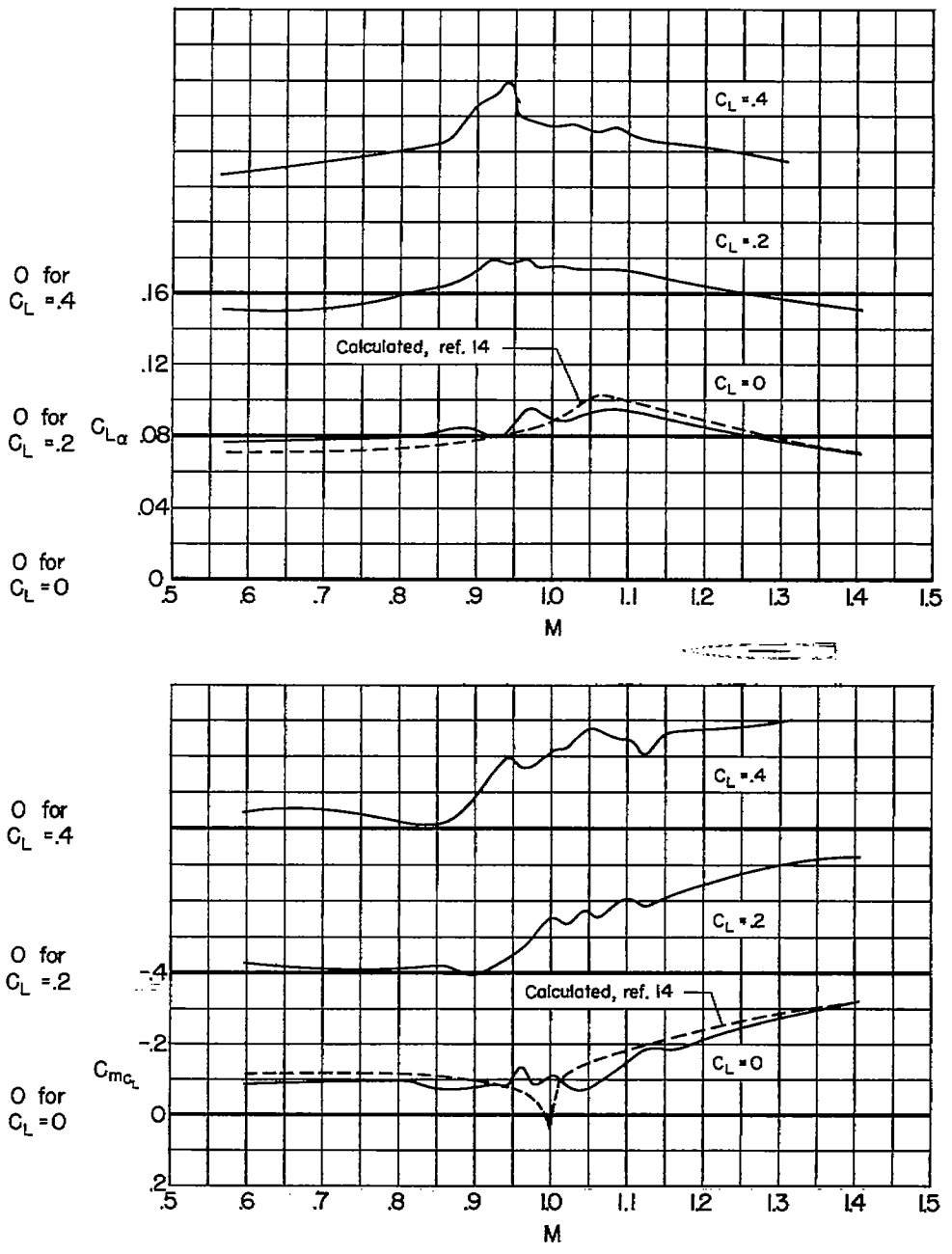

(b) Mid-wing, moderately high tail configuration; transition free.

Figure 11.- Continued.

[redacted]

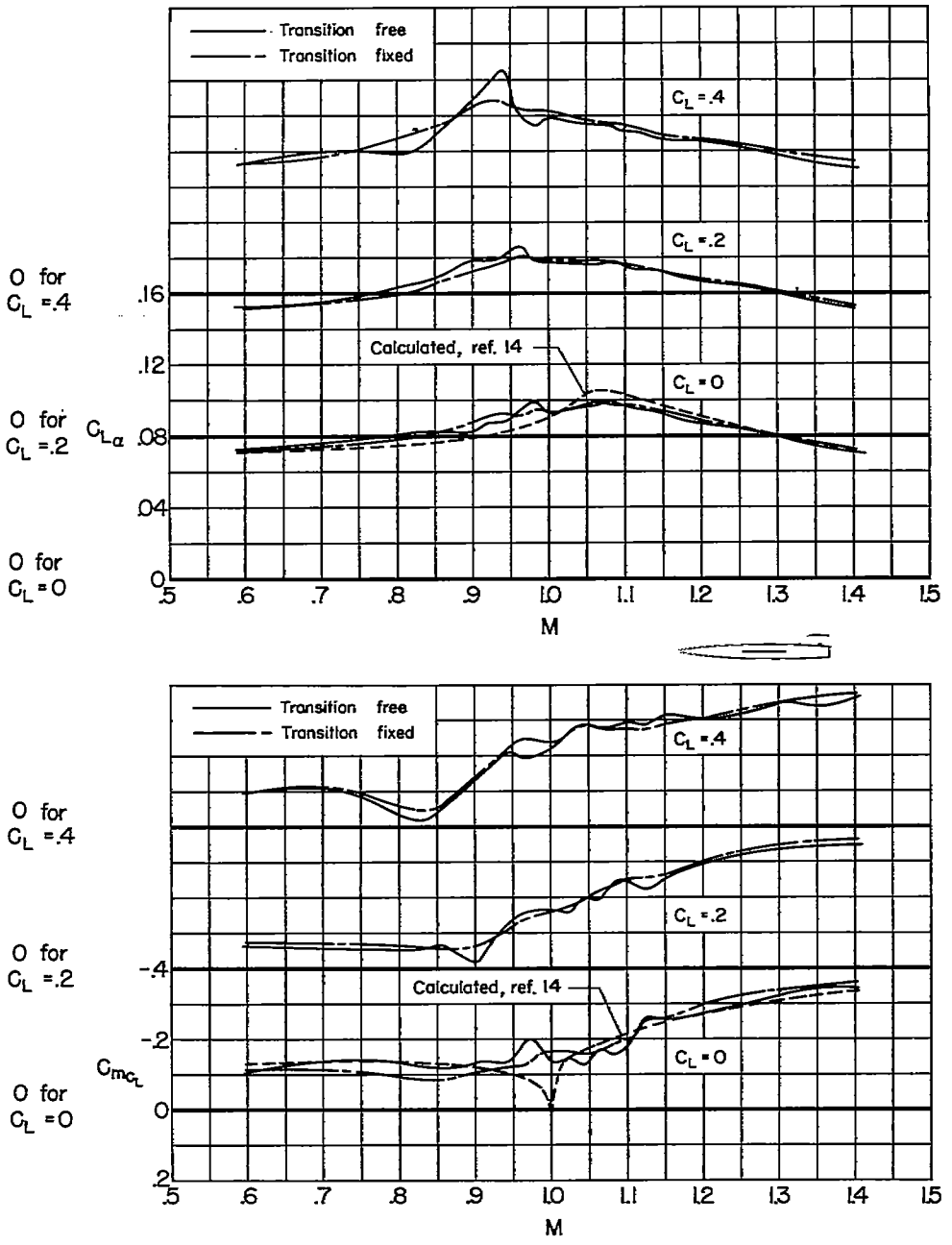

(c) Mid-wing, high-tail configuration.

Figure 11.- Continued.

[redacted]

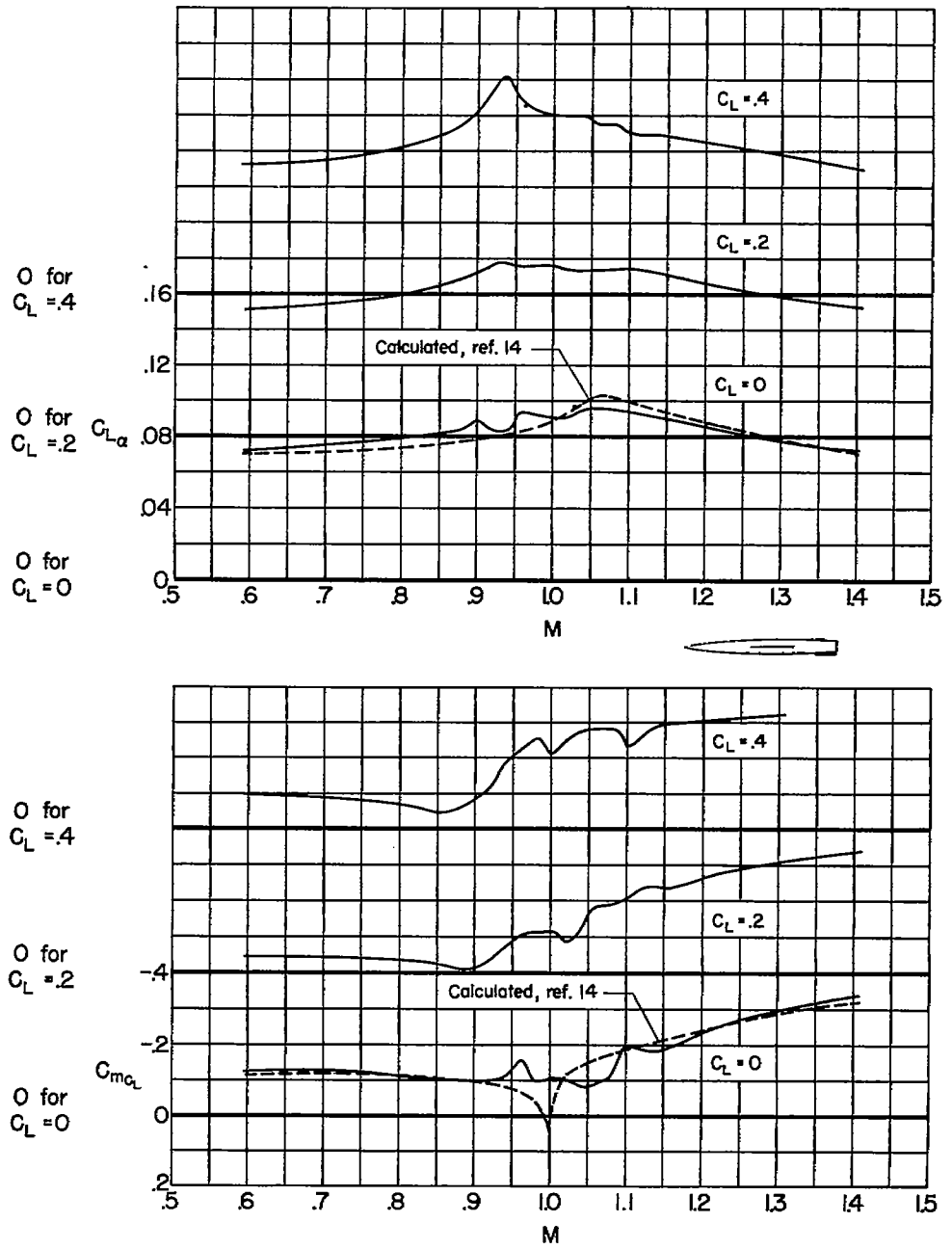

(d) Mid-wing, moderately low tail configuration; transition free.

Figure 11.- Continued.

[redacted]

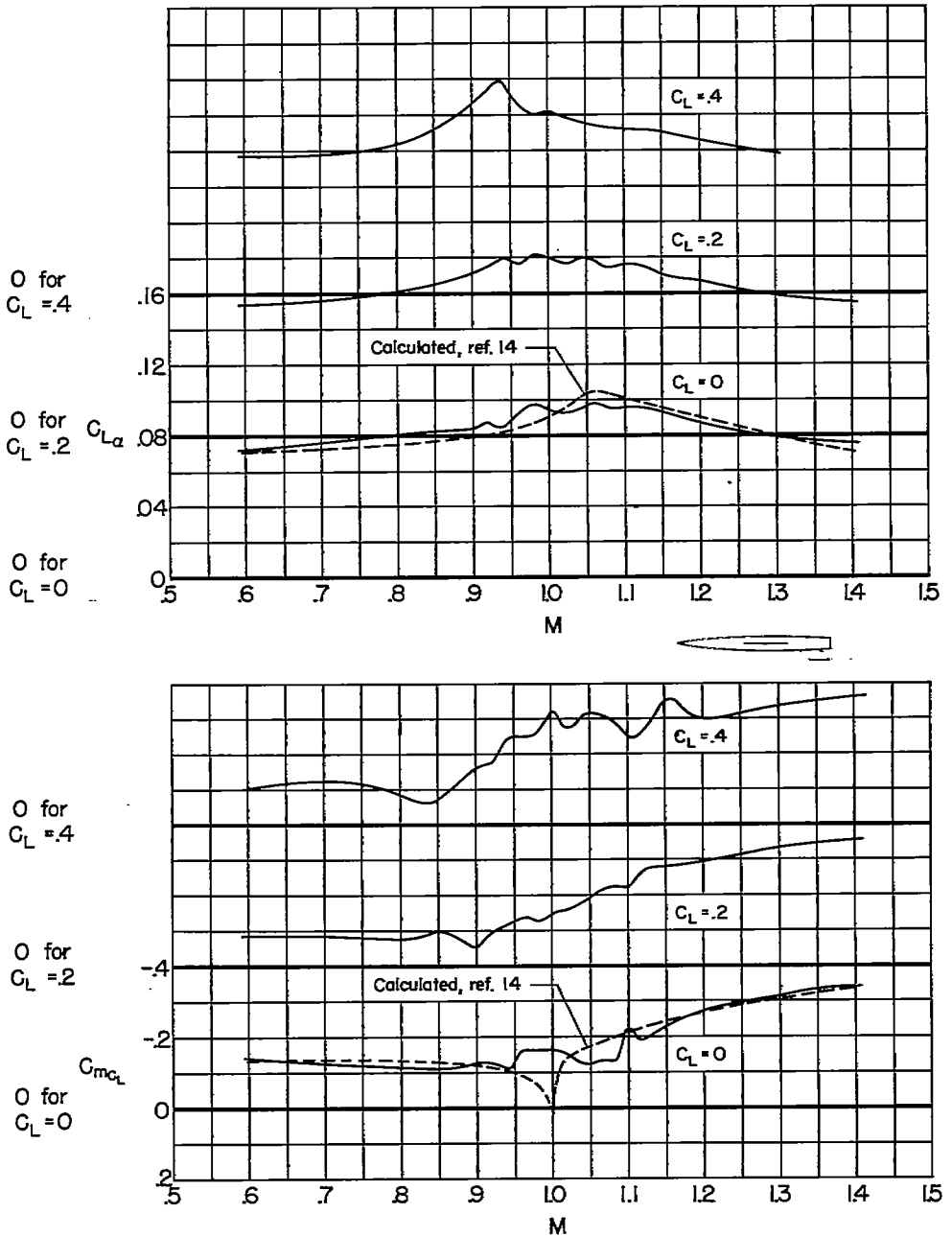

(e) Mid-wing, low-tail configuration; transition free.

Figure 11.- Continued.

[redacted]

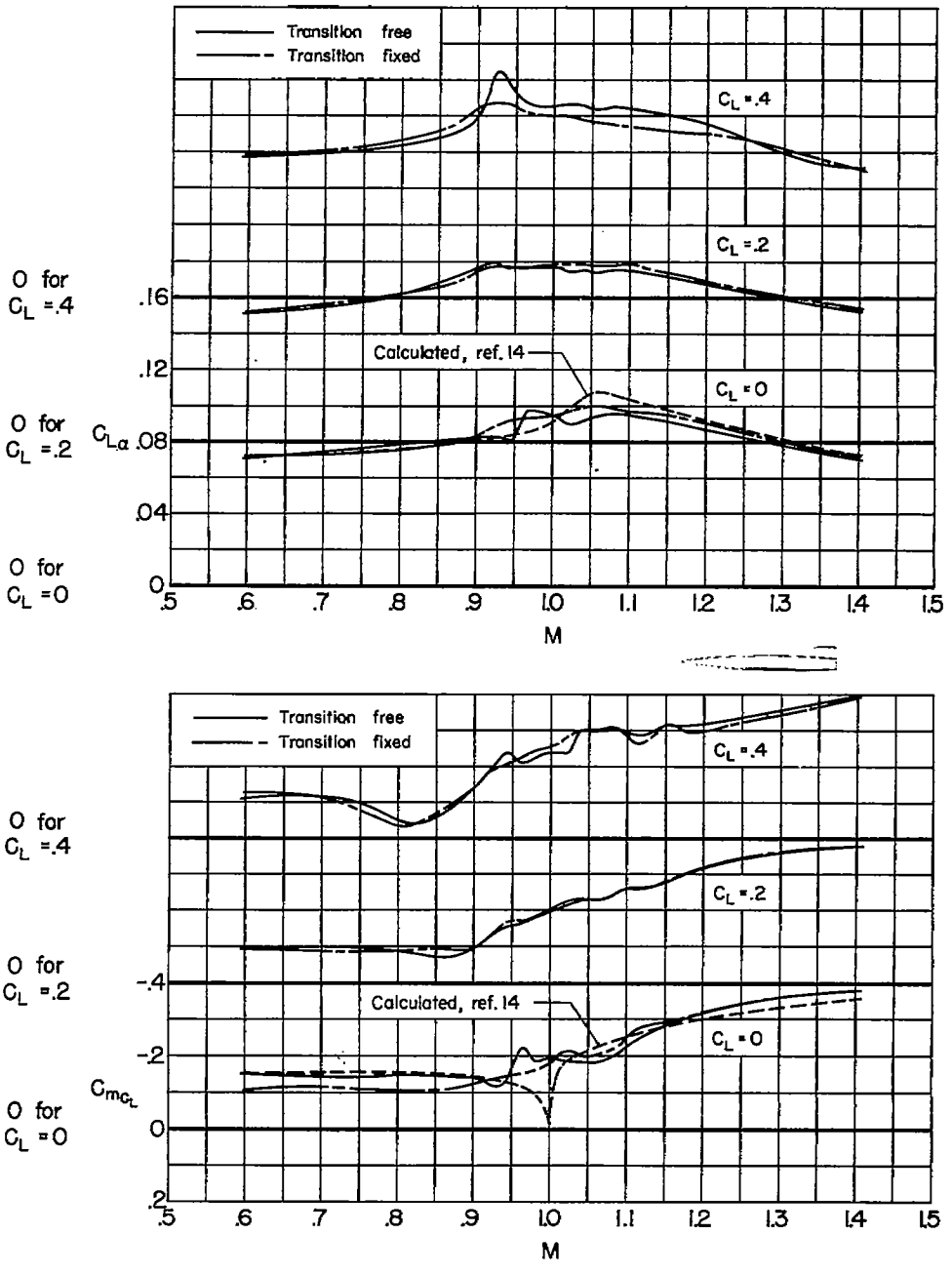

(f) Low-wing, high-tail configuration.

Figure 11.- Continued.

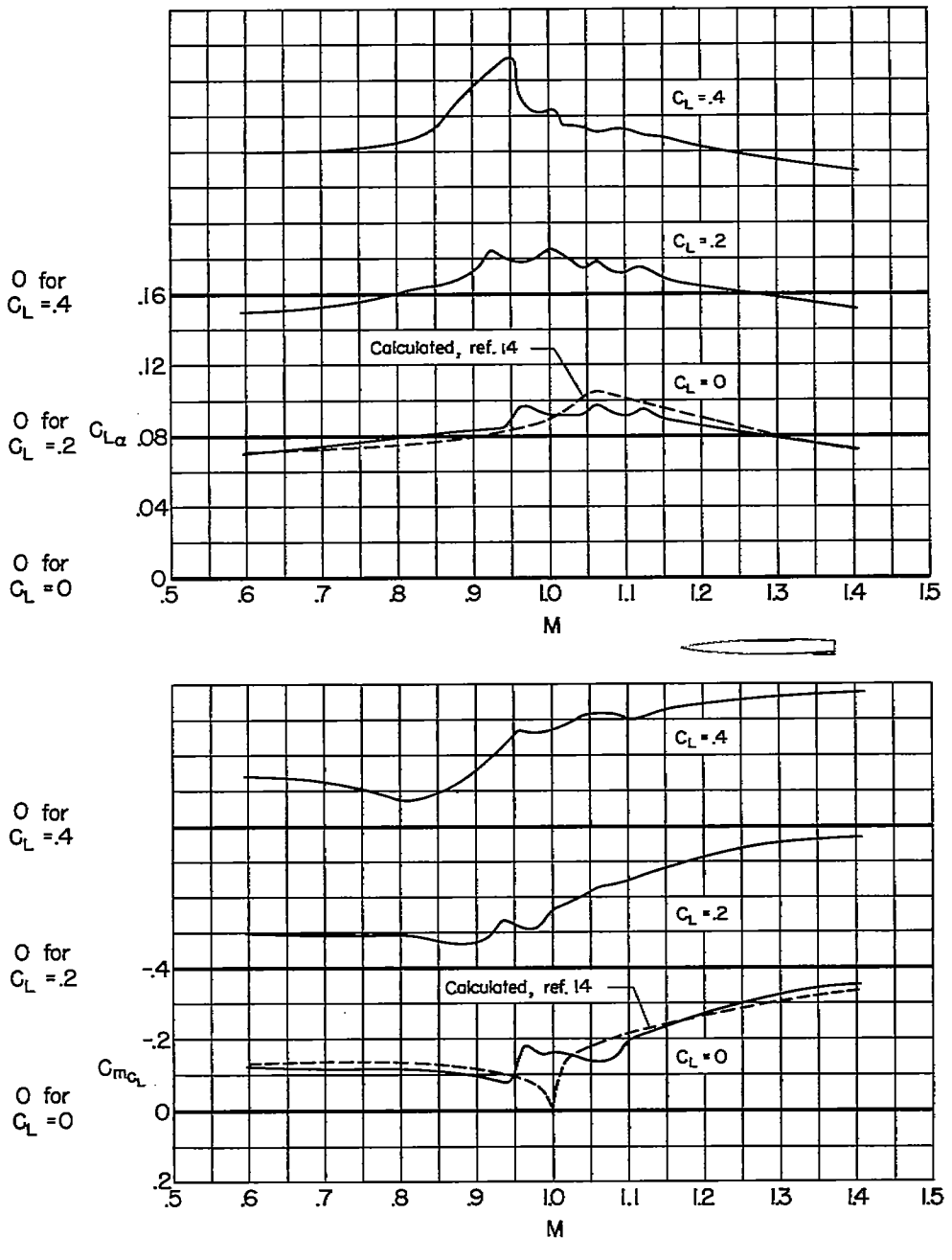

(g) High-wing, moderately low tail configuration; transition free.

Figure 11.- Concluded.

[redacted]

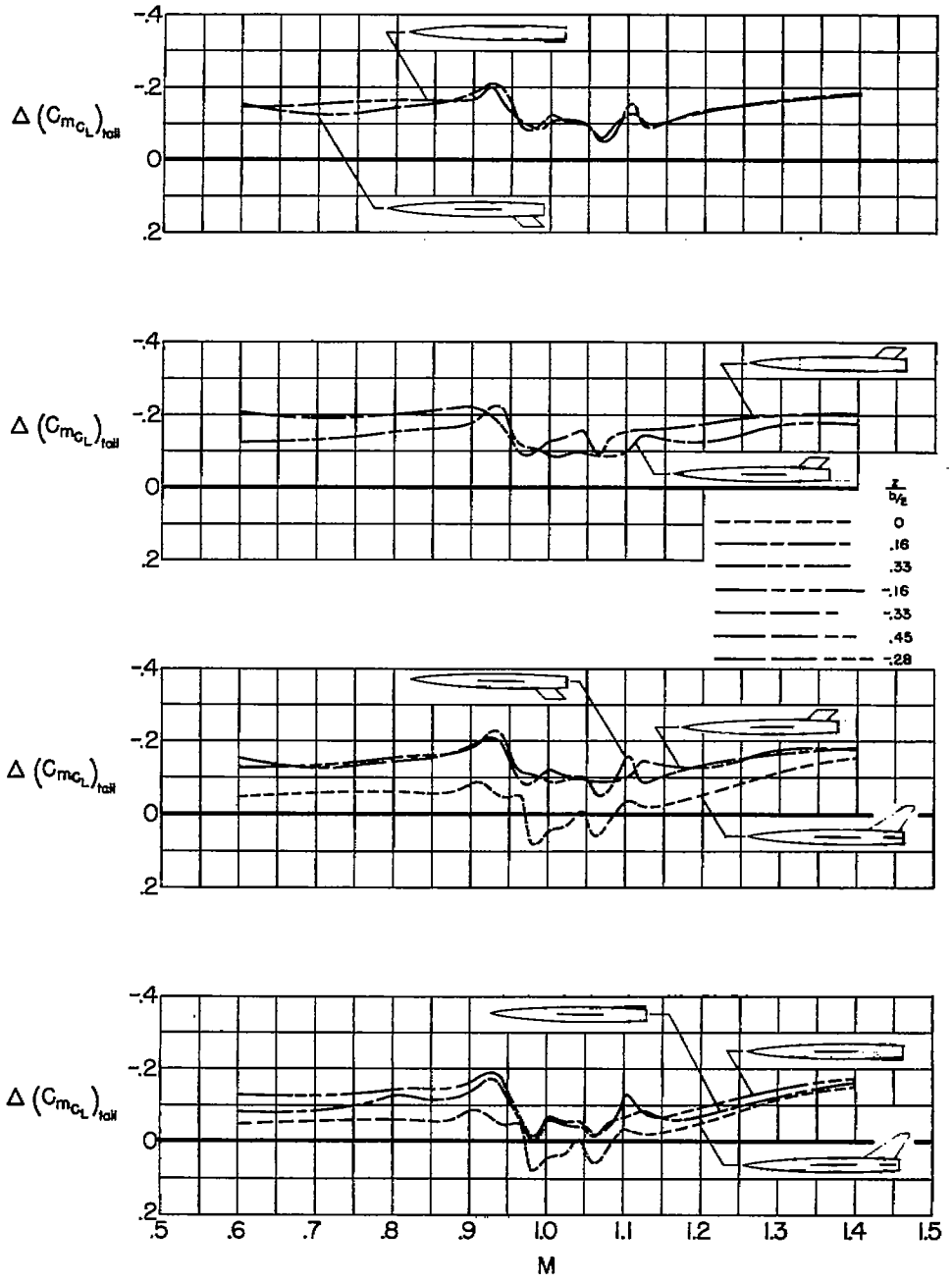

(a) Angle of attack for tail-off lift coefficient of zero.

Figure 12.- Effect of Mach number on the contribution of the horizontal tail to $C_{m_{C_L}}$; boundary-layer transition free.

[redacted]

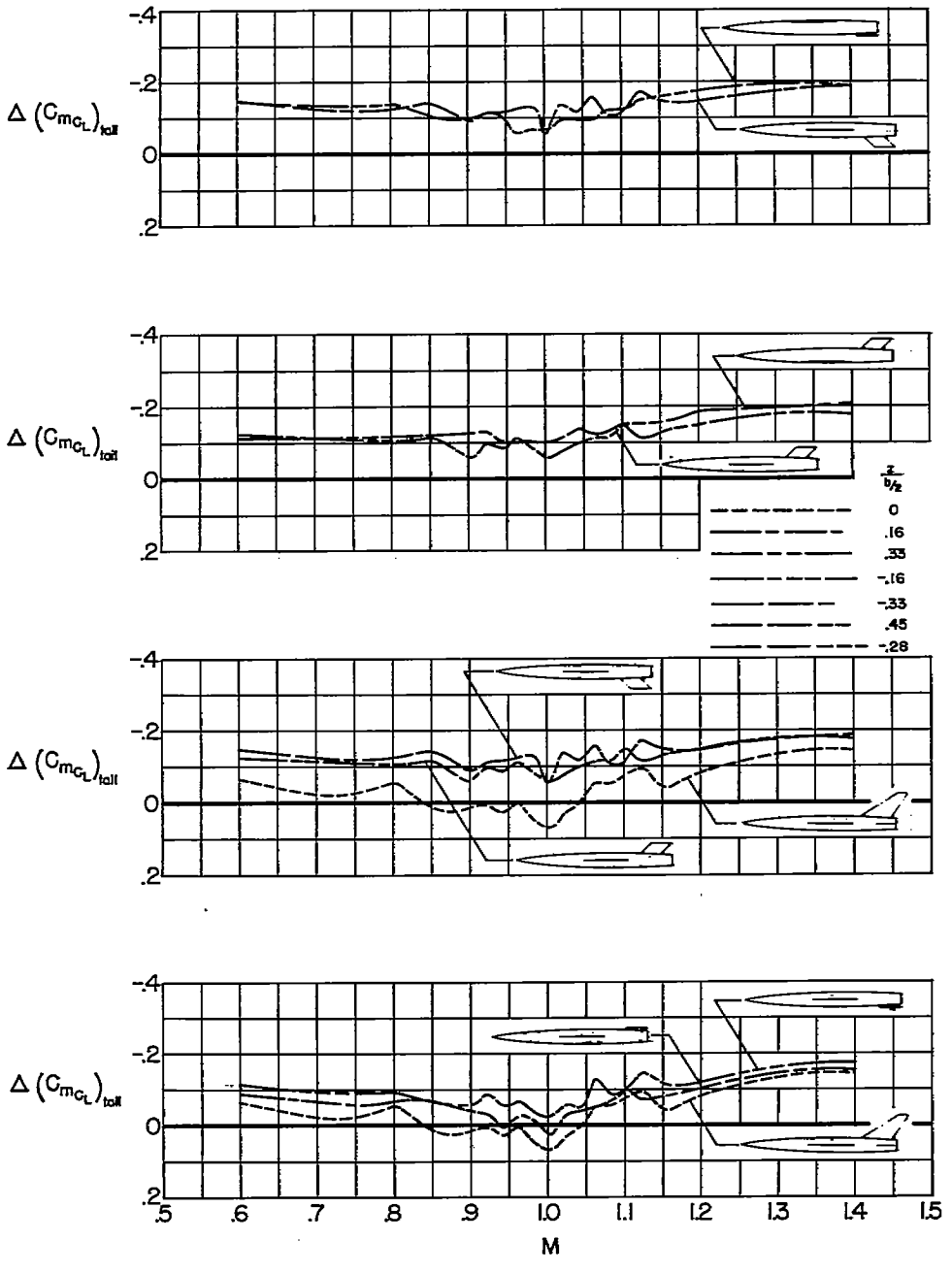

(b) Angle of attack for tail-off lift coefficient of 0.2.

Figure 12.- Continued.

[redacted]

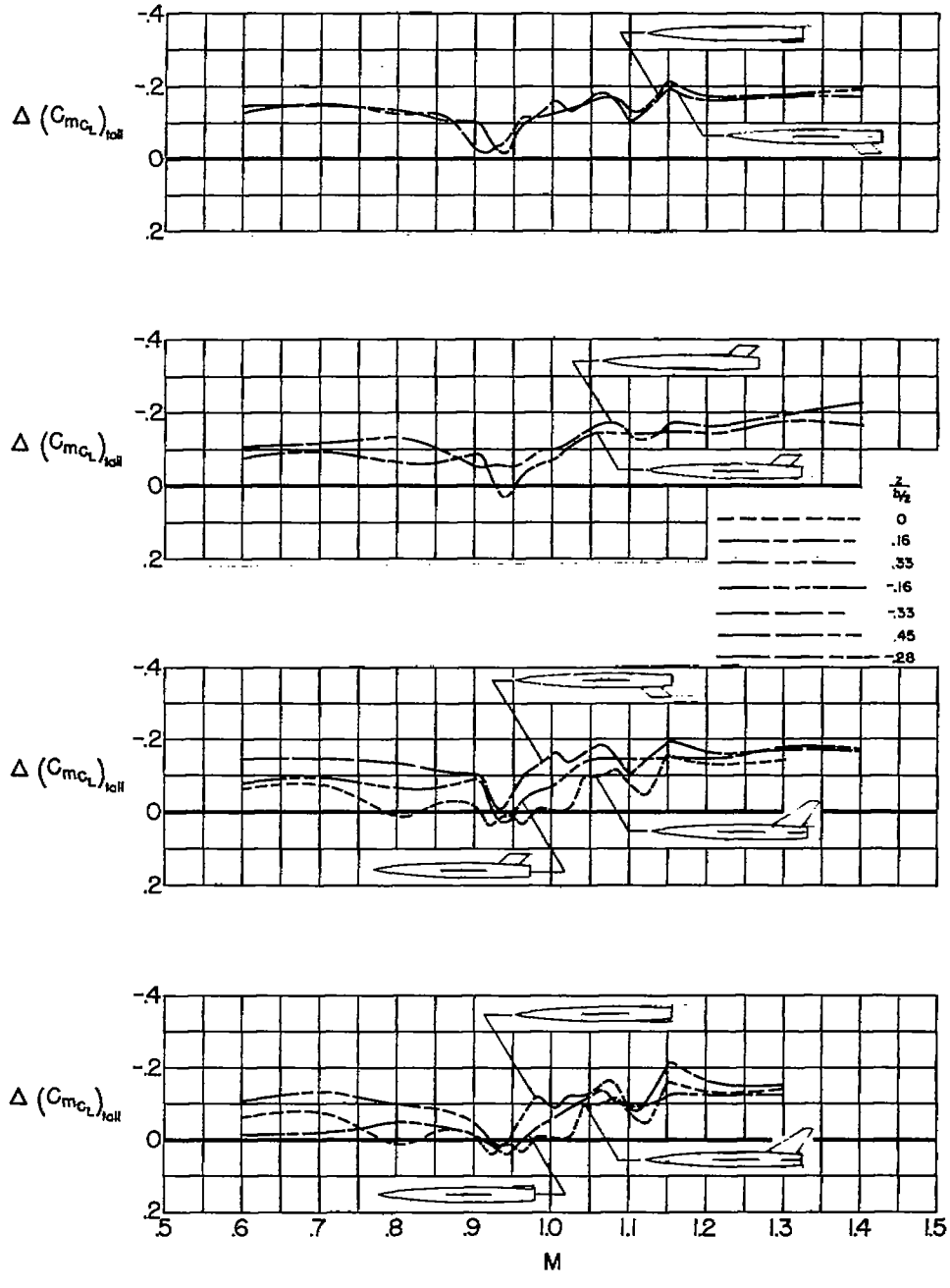

(c) Angle of attack for tail-off lift coefficient of 0.4.

Figure 12.- Concluded.

[redacted]

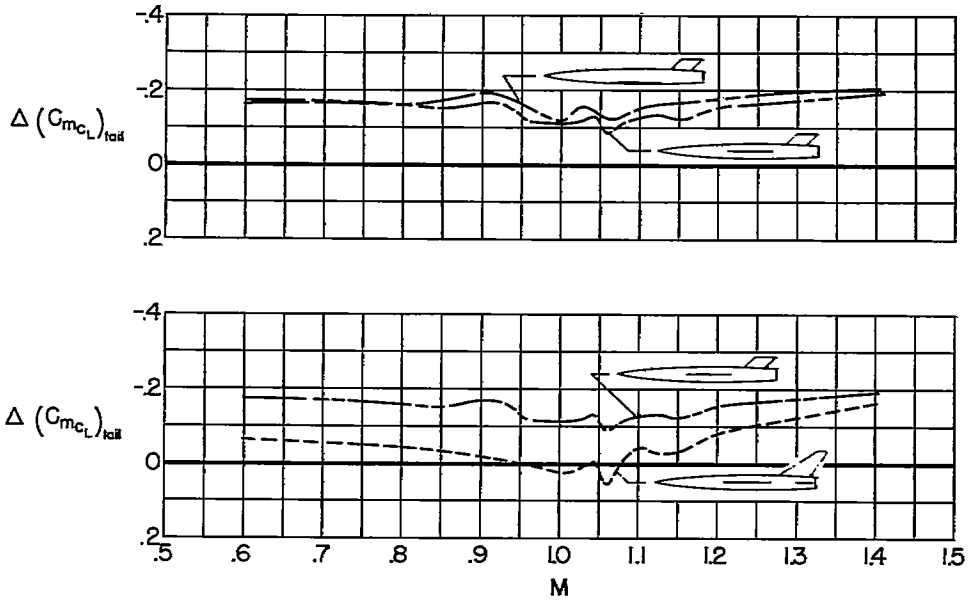

(a) Angle of attack for tail-off lift coefficient of zero.

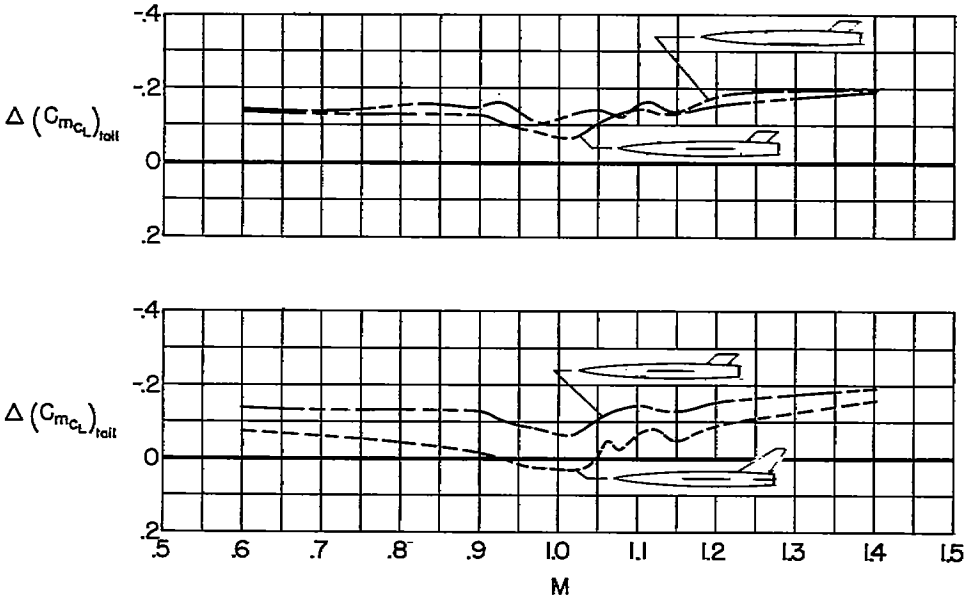

(b) Angle of attack for tail-off lift coefficient of 0.2.

Figure 13.- Effect of Mach number on the contribution of the horizontal tail to $C_{m_{C_L}}$; boundary-layer transition fixed.

[redacted]

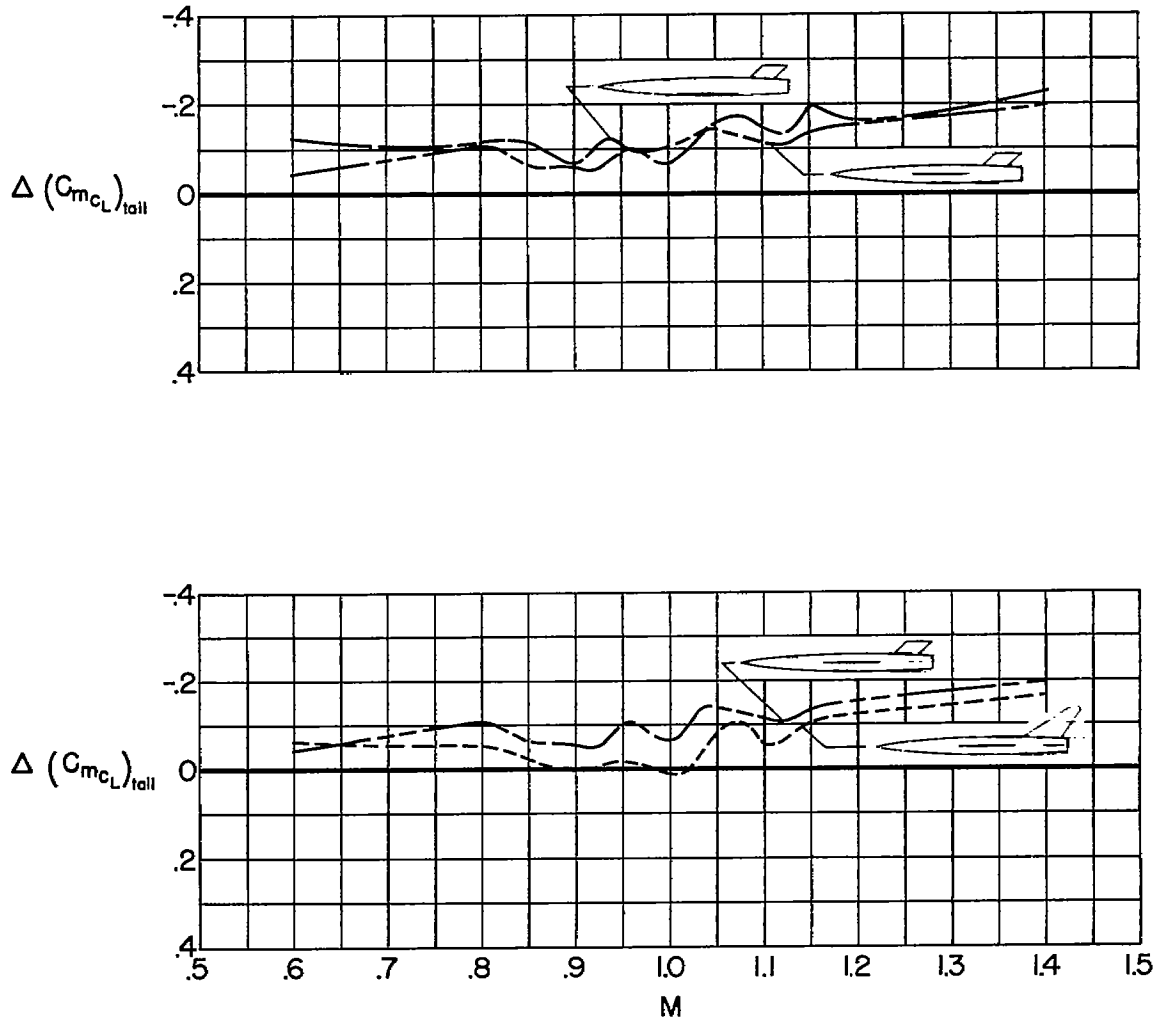

(c) Angle of attack for tail-off lift coefficient of 0.4.

Figure 13.- Concluded.

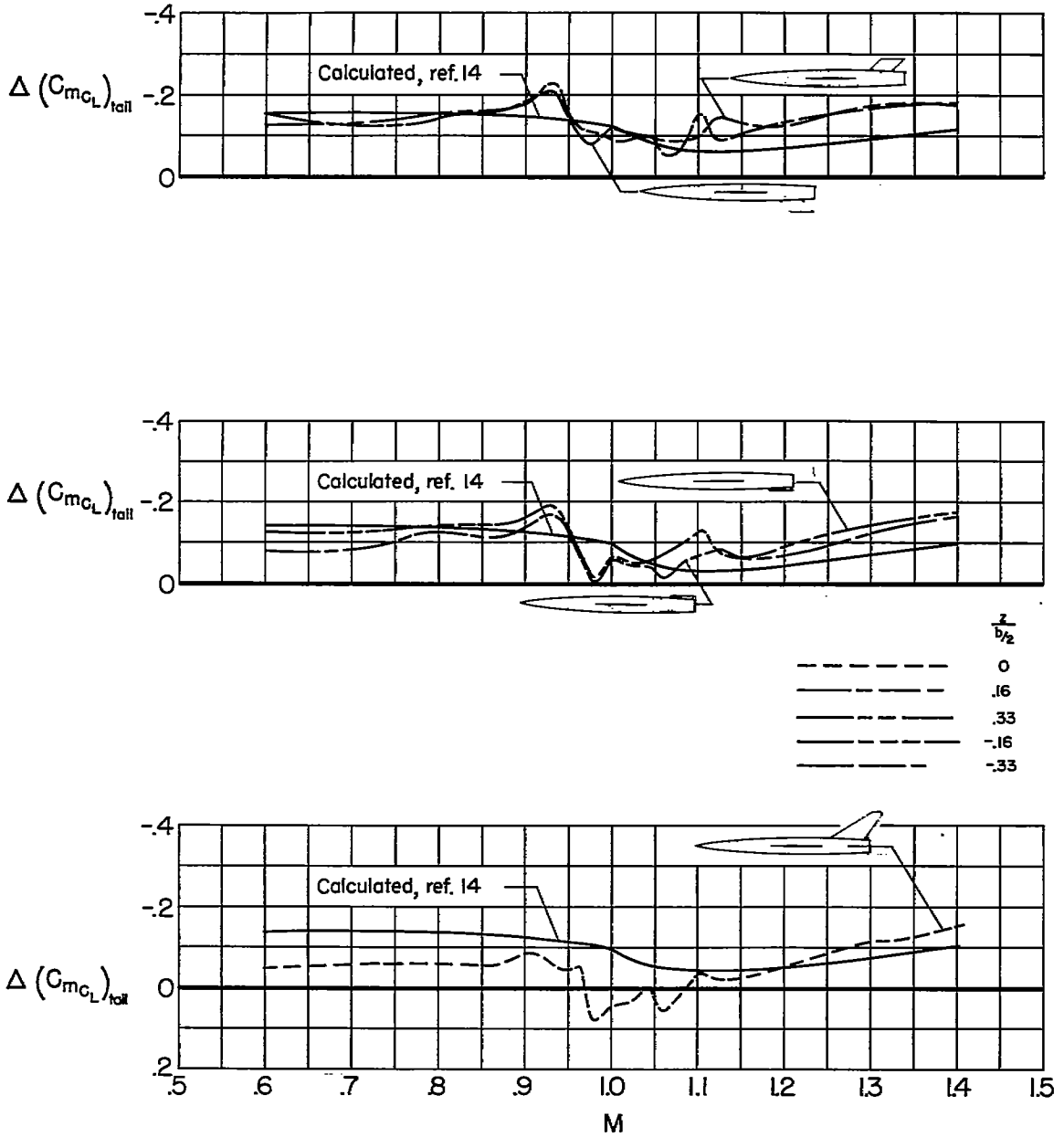

(a) Mid-wing configurations.

Figure 14.- Calculated and experimental values of the contribution of the horizontal tail to $C_{m_{C_L}}$ at an angle of attack for tail-off lift coefficient of zero; boundary-layer transition free.

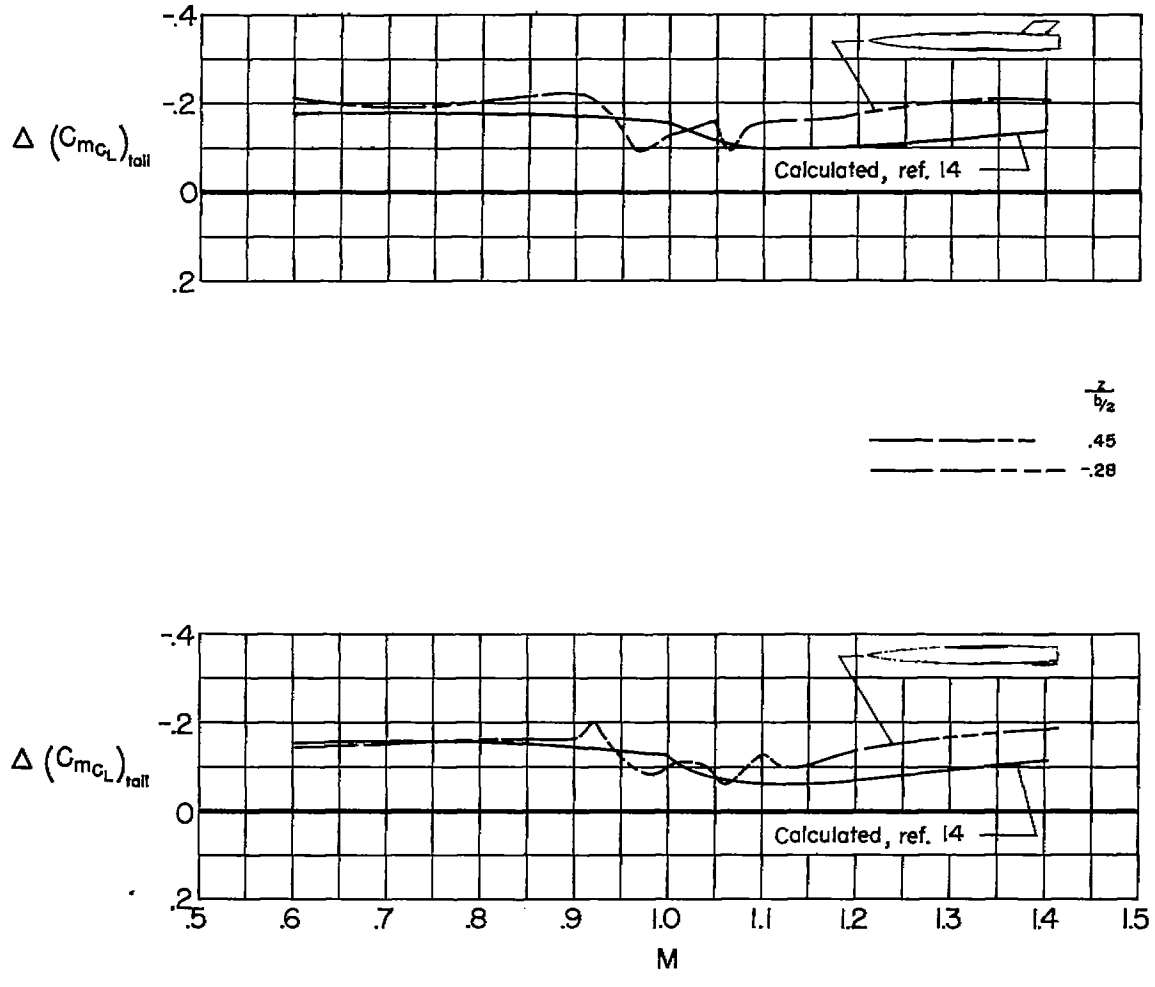

(b) Low- and high-wing configurations.

Figure 14.- Concluded.

NACA - Langley Field, Va.